

# Cretaceous mountain building processes triggered the aridification and drainage evolution in east Asia

Chihua Wu<sup>1,2,†</sup>, Xiaoming Sun<sup>3,4,†</sup>, Guangwei Li<sup>5</sup>, Leqing Huang<sup>6</sup>, Haijing Jiao<sup>7</sup>, Zhiwu Li<sup>1</sup>, Xing Jian<sup>8</sup>, Cody C. Mason<sup>9</sup>, and Juan Pedro Rodríguez-López<sup>2,10,11</sup>

<sup>1</sup>State Key Laboratory of Oil and Gas Reservoir Geology and Exploitation, Chengdu University of Technology, Chengdu 610059, China

<sup>2</sup>PAGODA Research Group (Plateau & Global Desert Basins Research Group), Institute of Sedimentary Geology, Chengdu University of Technology, Chengdu 610059, China

<sup>3</sup>School of Marine Sciences, Sun Yat-sen University, Guangzhou 510006, China

<sup>4</sup>Guangdong Provincial Key Laboratory of Marine Resources and Coastal Engineering, Guangzhou 510006, China

<sup>5</sup>School of Earth Sciences and Engineering, Nanjing University, Nanjing 210023, China

<sup>6</sup>Hunan Institute of Geology Survey, Changsha 410116, China

<sup>7</sup>Southern Marine Science and Engineering Guangdong Laboratory (Zhuhai), Zhuhai 519082, China

<sup>8</sup>State Key Laboratory of Marine Environmental Science, College of Ocean and Earth Sciences, Xiamen University, Xiamen 361005, China

<sup>9</sup>Department of Geosciences, University of West Georgia, Callaway Building, 1601 Maple St., Carrollton, Georgia 30118, USA

<sup>10</sup>Department of Geology, Faculty of Science and Technology, University of the Basque Country (UPV/EHU), Ap. 644, E-48080 Bilbao, Spain

<sup>11</sup>Permafrost Laboratory, Department of Geography, University of Sussex, Brighton BN1 9QJ, UK

## ABSTRACT

Knowledge of the late Mesozoic topography and drainage system of the Tibetan Plateau is essential for understanding the Cenozoic tectonic dynamics of the plateau. However, systematic analyses of the pre-Cenozoic surface uplift history and sediment-routing systems of the Tibetan Plateau remain sparse. Here we present new results for paleocurrents and U-Pb detrital zircon geochronology from the Lanping Basin, a key junction in the southeastern (SE) Tibetan Plateau, and integrate multidisciplinary data sets to constrain sediment provenance and reconstruct paleotopography and its drainage system throughout the Cretaceous. Our results indicate that mid- to Late Cretaceous (ca. Albian–Santonian) tectonically induced surface uplift occurred in the SE Tibetan Plateau, leading to the build-up of an extensive topographic barrier, and resultant rain shadows in the interior of east Asia. Superimposition of this topographic pattern by uplands in the eastern margin of Asia meant that the Cretaceous topography of east Asia was characterized by an enclosed paleo-relief pattern that was high in both the east and west, with drainage

from the east and west to the south, contrasting with previously proposed configurations. This topographic pattern interrupted the atmospheric circulation pattern and generated widespread intracontinental desertification and drainage network evolution in east Asia. Our study constrains a key part of the late Mesozoic growth of the Tibetan Plateau prior to the Cenozoic collision between India and Eurasia and will improve our understanding of the paleoclimate, atmospheric circulation, and modern drainage system evolution of the east Asian continent.

## INTRODUCTION

Surface uplift of the Tibetan Plateau has long been considered to be a direct result of the India-Eurasia collision during the Cenozoic (Dewey et al., 1988; England and Houseman, 1988; Ruddiman and Kutzbach, 1989; Tapponnier et al., 2001; Wang et al., 2008; van Hinsbergen et al., 2012; Meng et al., 2012, 2017; Molnar, 2018; Spicer et al., 2021). This continent-continent collision event and resultant topographic uplift are believed to have had an impact on the atmospheric circulation pattern of the Northern Hemisphere and to have stimulated the Asian monsoon system (Ruddiman and Kutzbach, 1989; Farnsworth et al., 2019; Spicer et al., 2021). The formation of this large-scale high stepped landform and the Paratethys retreat have been proposed triggers of the aridification of the

interior of east Asia (Guo et al., 2002; Sun et al., 2010; Bosboom et al., 2014; Carrapa et al., 2015; Wang et al., 2019; Sun et al., 2020), although, in contrast, the major drainage systems of the Asian continent are currently understood to have evolved within the framework of the tectonically induced uplift of the Tibetan Plateau during the Cenozoic (Clark, et al., 2004; Zheng, 2015; Chen et al., 2017; Zhao et al., 2021).

Owing to the existence of Cretaceous coastal mountains and eastern plateaus (Chen, 2000; Wu et al., 2018; Suo et al., 2019; Cao et al., 2020), the late Mesozoic paleotopography of east Asia has been generally considered to have been elevated in the east while low in the west, and may not have shifted to a reversed pattern until the Cenozoic India-Eurasia collision occurred (Wang, 1998). However, recent recognition of cryospheric processes on the Cretaceous plateau-desert oases of SE Tibet suggests an already uplifted plateau before the India-Eurasia collision in the western South China Block and the northern Indochina Block (Wu and Rodríguez-López, 2021). Actually, various studies have confirmed that there were extensive mountain systems or even plateaus in the east Asian interior during the mid- to Late Cretaceous, specifically in the SE Tibetan Plateau area (Wu et al., 2022), including the possible existence of landforms referred to as the initial Tibetan Plateau (Xu et al., 2016), or the Zoige Plateau (Liu et al., 2019), and the Gangdese Mountains (Kapp and Decelles, 2019; Meng et al., 2018, 2019, 2020;

Chihua Wu  <https://orcid.org/0000-0002-4244-8626>

<sup>†</sup>wuchi-hua@foxmail.com; eessxm@mail.sysu.edu.cn

Ding et al., 2022). On the landward side of these uplands, sedimentary records suggest extensive long-lasting aridification processes occurred, accompanied by the formation of widespread ergs and playas (Wu et al., 2017, 2022; Li et al., 2018a, 2018c; Rodríguez-López and Wu, 2020; Wang et al., 2023). Moreover, almost all of the Cretaceous intracontinental basins in the SE Tibetan Plateau record widespread coeval aqueous to eolian sedimentary systems and paleoclimatic transition events (Wu et al., 2017, 2022; Li et al., 2018a, 2018c), which occurred around the time of regional magmatic and tectonic activity (Hou et al., 2001; Reid et al., 2005; Wilson and Fowler, 2011; Wang et al., 2014; Xu et al., 2016; Liu et al., 2019; Wang et al., 2021). However, although the links between the evolution of tectonism, climate, and geomorphology have been recently elucidated (Wu et al., 2022), there is a gap in the knowledge of how tectonic dynamics during the Cretaceous influenced the hydrologic evolution of the SE Tibetan Plateau area.

The Lanping Basin (LPB; Fig. 1) developed in a key junction of several blocks (the Indochina and South China blocks, the eastern Songpan–Ganzi Complex, and the Yidun Arc), and contains exceptional Cretaceous stratigraphic successions that record environmental variations in response to changes in the topography and climate of the SE Tibetan Plateau (Schärer et al., 1990; Burchfiel and Chen, 2013; Li et al., 2018a). In addition, the completed Cretaceous stratigraphic sequences and detrital zircon age data set from the Sichuan Basin can also be used for comprehensive comparative study of paleoenvironment and provenance analysis (Li et al., 2018c). The aim of this work is to understand from a multiproxy analysis whether the pre-Cenozoic mountain building processes had an impact on the paleotopography and drainage basin hydrology of the SE Tibetan Plateau before the collision of India and Eurasia. For this, we apply several main approaches, including: (1) to combine sedimentological and paleocurrent data sets with detrital zircon U–Pb geochronology of Cretaceous rocks from the LPB, integrating them with previous results for other basins on the SE Tibetan Plateau; (2) to use three-dimensional multidimensional scaling analysis (3-D MDS) and detrital zircon U–Pb age unmixing modeling to constrain the provenance of the Cretaceous windblown and water-lain sediments; and (3) to

integrate these data sets with other multidisciplinary data sets, such as low-temperature thermochronology and tectonic-magmatic data sets. Further, we discuss the co-evolutionary mechanisms of tectonics, climate, and geomorphology, and examine paleoclimatic variation and rain-shadow migration in east Asia throughout the Cretaceous.

## GEOLOGICAL SETTING

The SE Tibetan Plateau consists of several continental fragments, including parts of the Qiangtang, Lhasa, Indochina, and South China blocks, the eastern Songpan–Ganzi Complex, and the Yidun Arc (Fig. 1A) (Bally et al., 1980; Şengör, 1985; Yin and Harrison, 2000; Burchfiel and Chen, 2013). During the Late Permian–Triassic accretion of these blocks, several suture zones related to the closure of the Paleo-Tethys Ocean were formed (Metcalf, 2011). The SE Tibetan Plateau has undergone a complex deformation history that spans the Mesozoic and Cenozoic and developed a series of Mesozoic basins (Burchfiel and Chen, 2013), including the LPB, Sichuan Basin (SIB), Simao Basin, Chuxiong Basin, and Korat Basin (Figs. 1A and 1B; Fig. S1 in the Supplemental Material<sup>1</sup>). The LPB is located at the junction of the Indochina Block, the South China Block, the Songpan–Ganzi Complex, and the Yidun Arc (Schärer et al., 1990; Burchfiel and Chen, 2013), and is bounded by two large and deep faults, the Lancang River fault in the west and the Jinsha–Ailao–Red River fault in the east (Fig. 1B). The southern end of the LPB intersects with the Simao Basin, Vientiane Basin, and Korat Basin, jointly forming a large-scale lake chain-rift basin system during the late Mesozoic (Metcalf, 2011; Wang et al., 2021, 2023).

The LPB contains Cretaceous deformed red-bed successions of the Jingxing, Nanxin, and Hutousi formations, from bottom to top (see Fig.

<sup>1</sup>Supplemental Material. Stratigraphic division of Cretaceous in the SE Tibetan Plateau. Methods: Detrital zircon U–Pb results of Cretaceous in the Lanping Basin. Detrital zircon U–Pb signals of Cretaceous in the Sichuan Basin. Detrital zircon U–Pb signals of potential source areas. Figures S1–S5. Supplementary References. Please visit <https://doi.org/10.1130/GSAB.S.23800506> to access the supplemental material, and contact [editing@geosociety.org](mailto:editing@geosociety.org) with any questions.

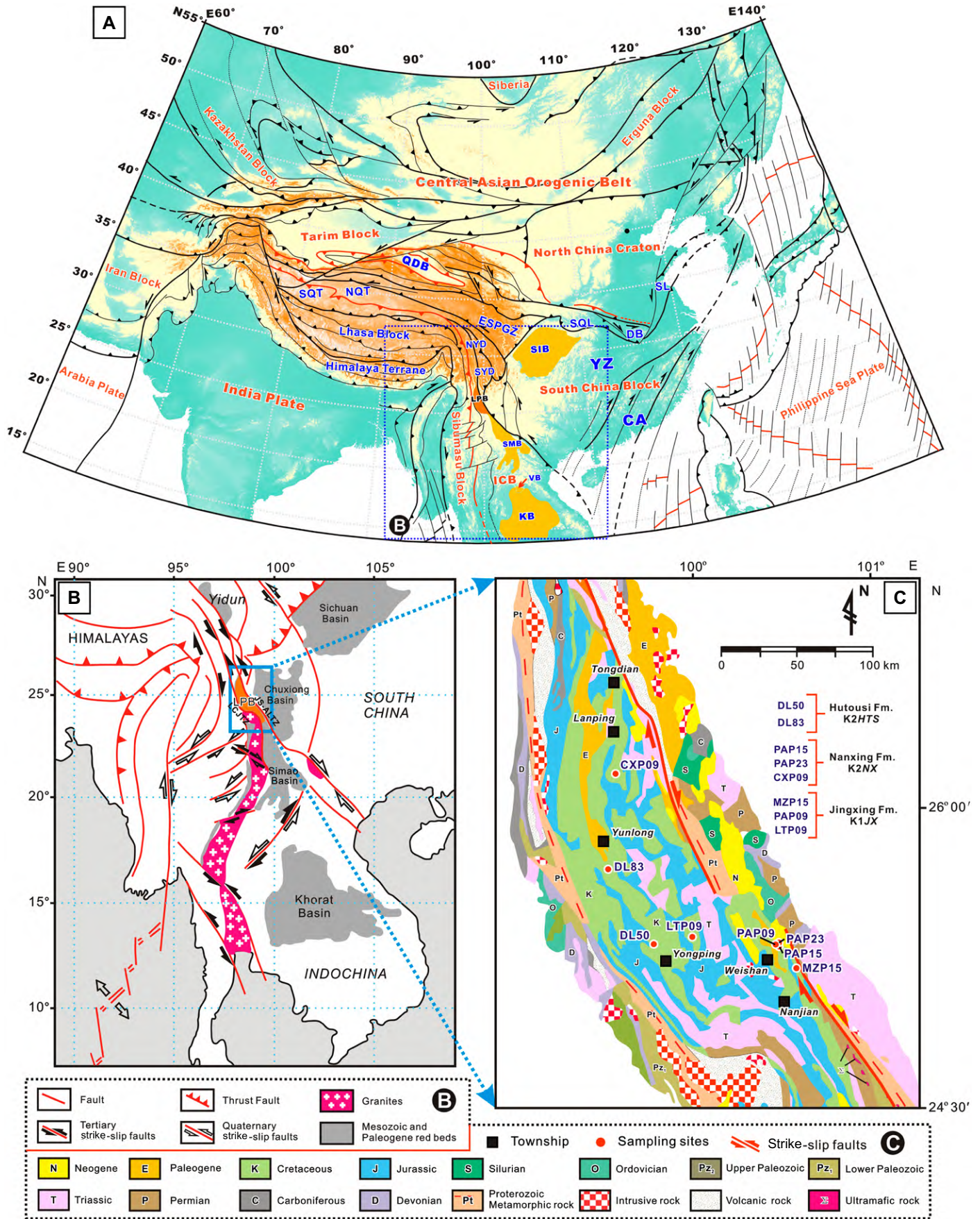
S1). The Jingxing Formation (Fm.) is dominated by red and grayish-green sandstones and mudstones of fluvial-lacustrine origin and contains Early Cretaceous fossils such as sporopollen (*Classopollis* sp.), Ostracoda (*Monosulcoocypris-Cypridea*), and lamellibranchs (*Cyotrigonioides-Nippononaia-Plicatounio*) (Li et al., 2018a). The Nanxin Fm. consists of cross-bedded red sandstone deposited in an erg (aeolian sandy desert) system, whereas the Hutousi Fm. is characterized by yellowish-gray and purplish sandstones with cross-bedding, also indicating an eolian origin (Li et al., 2018a). The Nanxin and Hutousi formations have similar characteristics both in terms of their lithology and sedimentary environment origins as well as their lack of direct evidence of biological activity. Systematic magnetostratigraphic studies combined with the study of volcanic rock chronology have dated the Hutousi Fm. as a Late Cretaceous Coniacian–Santonian (89.8–83.6 Ma) unit, the Nanxin Fm. as a mid-Cretaceous Albian–Turonian (113–89.8 Ma) unit, and the Jingxing Fm. as an Early Cretaceous Hauterivian–Barremian unit (132.9–125 Ma) (see Fig. S1) (Yin et al., 1999; Yuan et al., 2013; Wang et al., 2015, 2023; Yan et al., 2021).

## MATERIALS AND METHODS

### Paleocurrent Analysis

Paleocurrent orientation data from the LPB have been collected from Cretaceous eolian and water-lain facies from cross-bedding, long-axis transverse imbrications in channel lag conglomerates, and asymmetric ripples (Figs. S2 and S3). A total of 206 groups of paleocurrent orientation data from 16 outcrops were measured (Fig. 2), comprising 74 groups of paleo-water flow data and 132 groups of paleo-wind data (including 20 groups we collected in the Changxing area (Li et al., 2018a). Paleocurrent orientation data were corrected for post-Cretaceous average clockwise rotation (37°) of the crust based on paleomagnetic results (see Tong et al., 2013; Li et al., 2018a). Paleo-wind flow data is principally used to identify the prevailing paleo-winds of the study area (Wu et al., 2017, 2018; Li et al., 2018a), while paleo-water flow data is applied to reconstruct the sediment-routing system (Weissel et al., 2010; Jian et al., 2019).

**Figure 1.** (A) Distribution of continental/micro-continental blocks in east Asia (after Li et al., 2018b). (B) Schematic tectonic map of southeastern Asia (modified from Li et al., 2018a). (C) Geological map of the Lanping Basin, showing sample locations of the present study. CA—Cathaysia Block; DB—Dabie orogen; ESPGZ—eastern Songpan–Ganzi Complex; Fm.—Formation; ICB—Indochina Block; JS-ALTZ—Jinsha–Ailao tectonic zone; KB—Khorat Basin; LCJTZ—Lancangjiang tectonic zone; LPB—Lanping Basin; NQT—North Qiangtang Block; NYD—North Yidun terrane; QDB—Qaidam Basin; SIB—Sichuan Basin; SL—Sulu orogen; SMB—Simao Basin; SQL—South Qinling orogen; SQT—South Qiangtang Block; SYD—South Yidun terrane; VB—Vientiane Basin; YZ—Yangtze Craton.



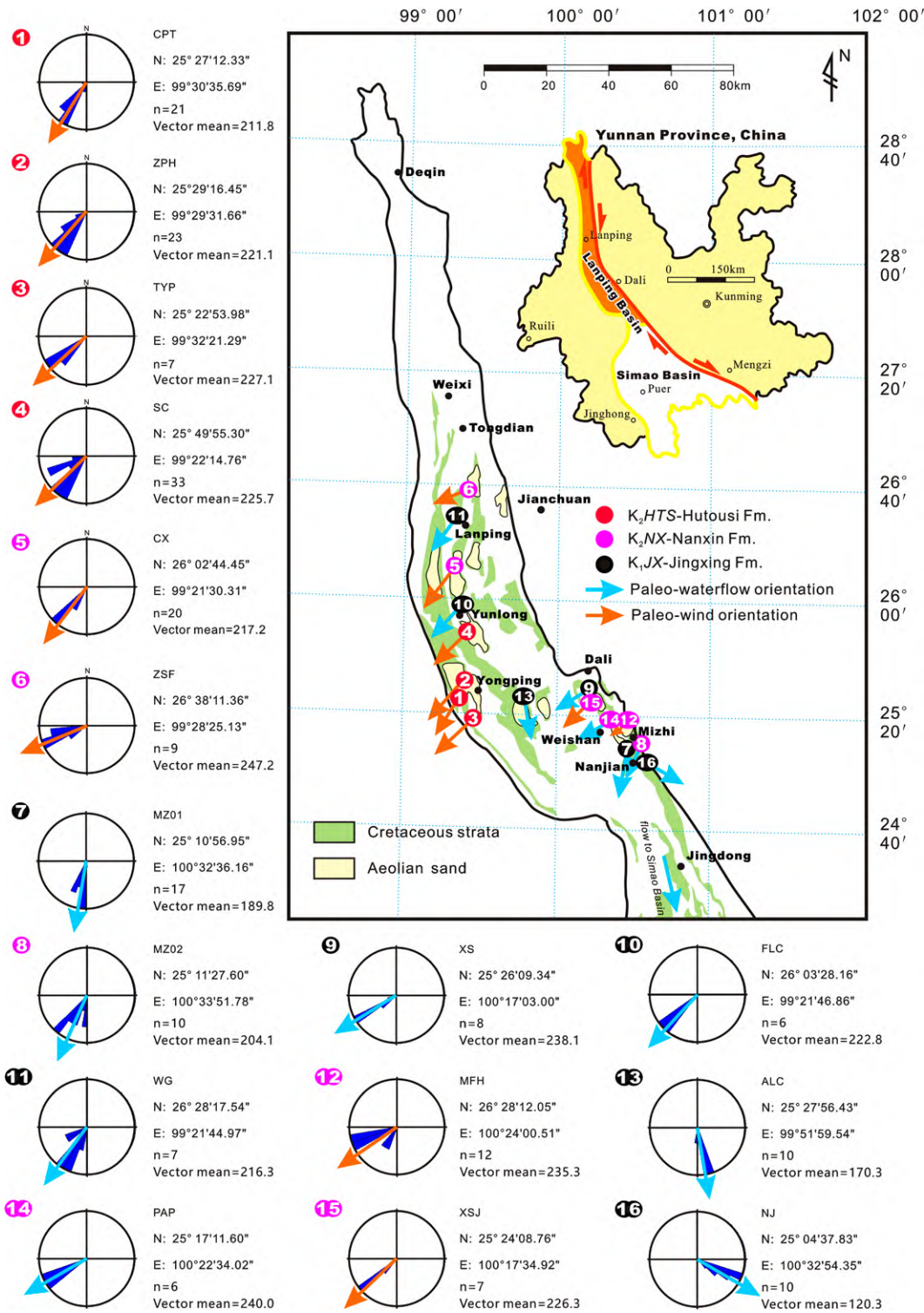


**Figure 2. Reconstruction of paleocurrent orientations in the Lanping Basin (LPB) in east Asia for the Cretaceous. Numbers indicate studied outcrops; arrows indicate paleocurrent orientations. The 16 outcrops from which paleocurrent data were obtained are as follows: 1—Changpingtan (CPT); 2—Zhuopanhe (ZPH); 3—Taoyuanpu (TYP); 4—Shicheng (SC); 5—Changxin (CX); 6—Zhongshuifeng (ZSF); 7—Mizhi (MZ01); 8—Mizhi (MZ02); 9—Xinsheng (XS); 10—Fenglianchang (FLC); 11—Wengu (WG); 12—Mofanghe (MFH); 13—Anlongchun (ALC); 14—Pinganzhuang (PAP); 15—Xiaosanxia (XSJ); 16—Nanjian (NJ). Fm.—Formation; n—number of paleocurrent orientations.**

**Sample Collection**

Eight samples were collected from Cretaceous rocks of the LPB for detrital zircon U-Pb geochronology analysis: three samples from the Jingxing Fm. (MZP15 from the Mizhi area; PAP09 from the Weishan area; and LTP09 from

the Yongping area), three from the Nanxin Fm. (PAP15 and PAP23 from the Weishan area; CXP09 from the Lanping area), and two from the Hutouzi Fm. (DX50 from the Yongping area; DX83 from Yunlong area) (Fig. 1C). Of these eight samples, those from the Jingxing Fm. are from fluvial deposits, while the rest are

aeolian facies. In terms of the formation process, these coarse aeolian sands are basically formed from the sediments of the alluvial-fluvial environment within the basin through aeolian reworking. So, the detrital zircon signal of aeolian sands can be used in provenance (source-to-sink) analysis.

## Detrital Zircon U-Pb Geochronology

All aspects of sample preparation, analysis, and data generation were conducted at Guangdong Provincial Key Laboratory of Marine Resources and Coastal Engineering, Guangzhou, China, where standard techniques of mineral separation and laser ablation–inductively coupled plasma–mass spectrometry U-Pb dating of zircon grains were used (see the Supplemental Material for details). A complete data set of isotopic measurements for detrital zircon U-Pb geochronology of the eight samples from the LPB is presented in Supplemental Data S1. Samples were divided into three groups according to stratigraphy: Groups  $K_1JX$ ,  $K_2NX$ , and  $K_2HTS$ . Results from these samples were combined with previous results for Groups  $K_1SC$ ,  $K_2JG$ , and  $K_2GK$  from the SIB (Li et al., 2018c) (see the Supplemental Material) to make six “daughter groups” (Fig. 2). In addition, to better constrain the potential provenances of these Cretaceous sandstones (daughter groups) from the LPB and SIB, available detrital zircon geochronological data from adjacent potential source areas (parent groups) were compiled as follows: the Jinsha-Ailao (JS-ALTZ), Lancangjiang (LCJTZ), and South Qinling (SQL) tectonic zones; the eastern Songpan–Ganzi Complex (north depocenter [N-ESPGZ], middle depocenter [M-ESPGZ], south depocenter [S-ESPGZ]); and the Qiangtang (Northern Qiangtang [NQT] and Southern Qiangtang [SQT]), Western Yangtze (W-YTZ), and Yidun Arc (North Yidun [N-YD] and South Yidun [S-YD]). Initial comparisons of detrital zircon U-Pb age distributions among parent groups and daughter groups were accomplished by visual inspection of the relative abundances of component (subpopulation) age groups (Fig. 3A).

### Eastern Songpan–Ganzi Complex (ESPGZ)

The ESPGZ is characterized by 5–10-km-thick Upper Triassic flysch and widespread Mesozoic granitoids (ca. 224–112 Ma, Roger et al., 2004, 2010; Zhang et al., 2006; Xiao et al., 2007; Weislogel, 2008; Yuan et al., 2010), with intense deformation and a large arc-shaped structural belt (Nie et al., 1994; Harrowfield and Wilson, 2005; Weislogel et al., 2006, 2010). The ESPGZ is not a single unified turbidite system, but consists of three relatively independent depocenters (Weislogel et al., 2010) (Fig. 3A). The N-ESPGZ depocenter contains a high density of ca. 256 Ma, ca. 469 Ma, ca. 1852 Ma detrital zircon ages with a minor portion of ca. 330 Ma and ca. 2498 Ma. The M-ESPGZ depocenter shows dominant age populations of ca. 267 Ma and ca. 443 Ma with few ca. 1876 Ma zircon while the S-ESPGZ depocenter predominates at ca. 1872 Ma with a minor portion of ca. 262 Ma, ca.

440 Ma, and ca. 740 Ma zircon (Weislogel et al., 2010). In addition, the M-ESPGZ and S-ESPGZ contain granite intrusions dated at 224–188 Ma and 228–112 Ma, respectively (Roger et al., 2004, 2010; Zhang et al., 2006; Xiao et al., 2007; Weislogel, 2008; Yuan et al., 2010).

### Yidun Arc (YD)

The YD comprises the Triassic Yidun Group flysch–volcanic succession and arc-related granite and granodiorite plutons with ages at ca. 245.2–75.8 Ma, integrally concentrating at ca. 86 Ma, ca. 215 Ma, and ca. 241 Ma (Hou et al., 2001; Reid et al., 2005; Wang et al., 2014; Weislogel, 2008; He et al., 2013). However, there are some differences between the detrital zircon ages of flysch–sediments in the south and north of YD (Fig. 3A). Detrital zircon ages of the Yidun Group in the N-YD fall into two prominent age populations of 490–400 Ma (ca. 440 Ma) and 2010–1790 Ma (ca. 1896 Ma), whereas the Yidun Group in the S-YD is characterized by a high density of ca. 261 Ma, ca. 424 Ma, and ca. 1885 Ma, with a minor portion of ca. 768 Ma and ca. 2476 Ma (Wang et al., 2014; Jian et al., 2019). By contrast, the N-YD contain granite intrusions dated at 238–76 Ma concentrating at ca. 86 Ma, while the age of granite intrusions in the S-YD concentrates at 245–80 Ma, and further concentrates at ca. 215 Ma and ca. 241 Ma.

### South Qinling Tectonic Zone (SQL)

The SQL is composed of Triassic granitoids (Li et al., 2015, and references therein), Paleozoic sediments (Dong et al., 2013), and Neoproterozoic volcanic and complex assemblage (Li et al., 2018c, and references therein). In general, the SQL is characterized by principal age populations of 245–189 Ma (with peak at ca. 221 Ma), 459–432 Ma (ca. 443 Ma), and 890–660 Ma (ca. 765 Ma), with a minor portion at 2550–2340 Ma (ca. 2496 Ma).

### Western Yangtze Craton (W-YTZ)

The W-YTZ consists of late Neoproterozoic plutonic complexes and sediments (Chen et al., 2013; Meng et al., 2015), Paleozoic sediments (Duan et al., 2011; Chen et al., 2018), and early to middle Mesozoic sediments (Zhu et al., 2017; Li et al., 2018c). In addition to these, the Late Permian Emeishan large igneous province is well exposed in the western margin of the Yangtze Block and yielded ages concentrating at ca. 261 Ma (Shellnutt, 2014, and references therein). As a whole, the W-YTZ is characterized by principal age populations of 300–210 Ma (with peak at ca. 261 Ma) and 1020–720 Ma (ca. 798 Ma), with minor portions at 690–420 Ma, 2010–1159 Ma (ca. 1860 Ma), and 2580–2310 Ma (ca. 2464 Ma) (Fig. 3A).

### North Qiangtang Block (NQT) and South Qiangtang Block (SQT)

The NQT contains abundant late Paleozoic–early Mesozoic and Precambrian zircon ages forming two prominent major populations at 304–228 Ma (with peak at ca. 259 Ma) and 1080–700 Ma (ca. 803 Ma), with smaller populations of Neoproterozoic (700–500 Ma), Paleoproterozoic (1920–1860 Ma), early Archean–early Paleoproterozoic (2610–2400 Ma), and 3566–2701 Ma (Gehrels et al., 2011) (Fig. 3A). The SQT is mainly dominated by Precambrian zircon ages forming several populations at 700–500 Ma (peaking at ca. 562 Ma), 1130–700 Ma (ca. 956 Ma), 2010–1780 Ma (ca. 1865 Ma), and 2650–2380 Ma (ca. 2471 Ma), with smaller populations of late Paleozoic–early Mesozoic 320–201 (ca. 262 Ma) (Gehrels et al., 2011) (Fig. 3A).

### Jinshajiang–Ailaoshan Tectonic Zone (JS-ALTZ)

The JS-ALTZ is principally composed of Silurian–Devonian and Triassic–Jurassic metasedimentary in the west and high-grade metamorphic rocks in the east (Liu et al., 2014; Wang et al., 2017). In addition, the magmatism related to the paleo-Tethys Ocean closure is widespread in the Jinshajiang–Ailaoshan suture zone and Lincang area. Along the Jinshajiang–Ailaoshan suture zone, zircons from volcanics and adakites range in age from 330 Ma to 211 Ma (with dominating populations at 245–211 Ma; Chen, 2017, and references therein). Generally, the JS-ALTZ is characterized by principal age populations of 300–213 Ma (peaking at ca. 246 Ma) and 470–390 Ma (ca. 443 Ma), and with minor portions at 1160–900 Ma and 2690–2430 Ma (Fig. 3A).

### Lancangjiang Tectonic Zone (LCJTZ)

The LCJTZ consists of Paleo-Tethys Ocean remnants associated with high-pressure metamorphic rocks, blueschist, and associated arc-magmatism (Wang et al., 2010, and references therein; Li et al., 2012; Chen, 2017, and references therein; Xu et al., 2018; Qi et al., 2019), Paleozoic sediments (Xin et al., 2018), and early to middle Mesozoic sediments (Shi, 2015). As a whole, the LCJTZ is characterized by principal age populations of 330–210 Ma (ca. 234 Ma) and 660–420 Ma (ca. 508 Ma), with minor portions at 1020–810 Ma (ca. 884 Ma), 1890–1590 Ma (ca. 1760 Ma), and 2580–2280 Ma (ca. 2448 Ma) (Fig. 3A).

### Three-Dimensional Multidimensional Scaling (3-D MDS)

Additional comparison of detrital zircon U-Pb age distributions was established using a

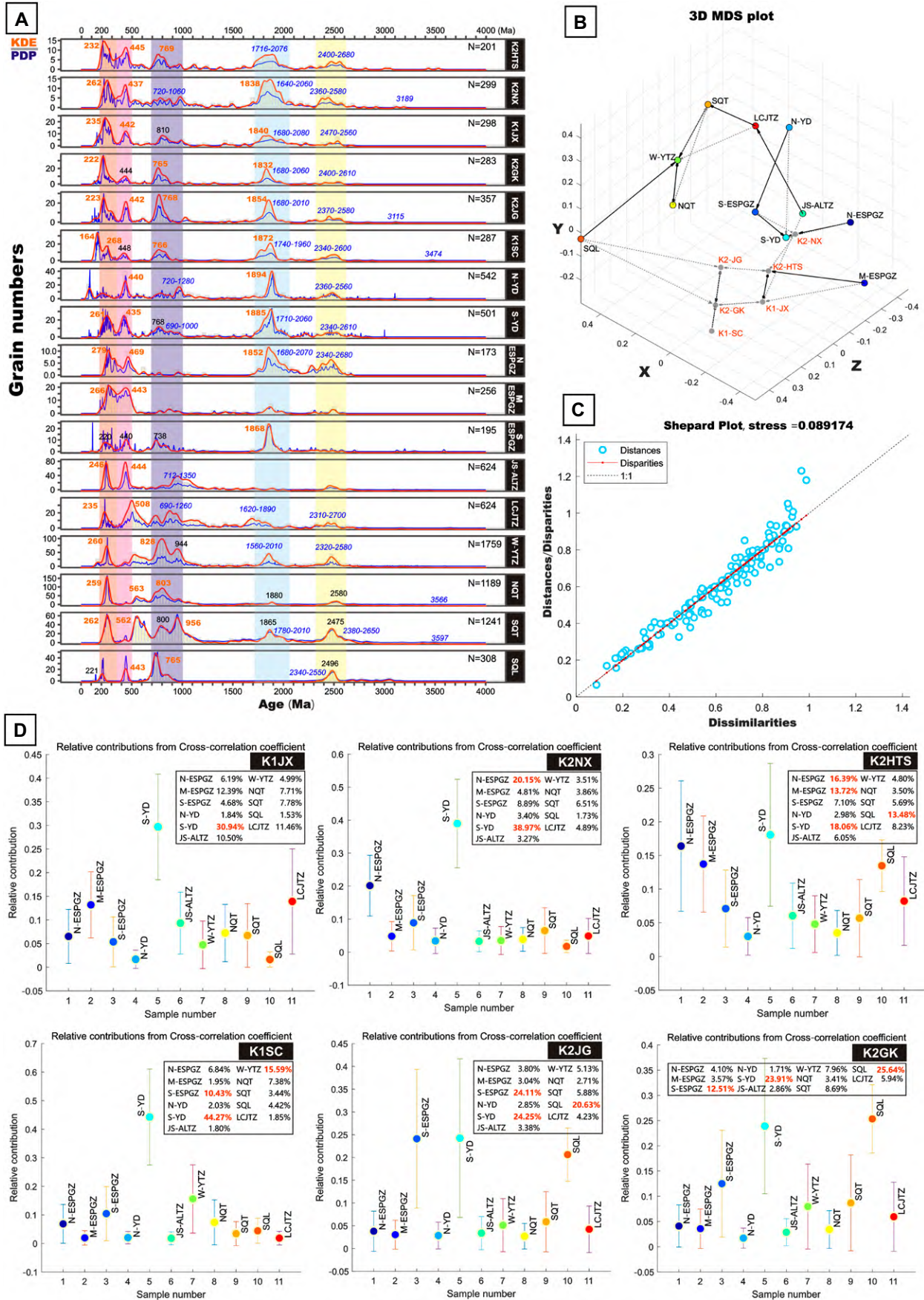


**Figure 3.** (A) Kernel density estimates (KDEs) and probability density plots (PDPs) of detrital zircon U-Pb ages from daughter groups in the Lanping Basin (this study), the Sichuan Basin (Li et al., 2018c), and potential source areas of study area (see the Supplemental Material [see text footnote 1] and references therein). (B) Three-dimensional multidimensional scaling analysis (3-D MDS) plot of daughter groups in the Lanping Basin, Sichuan Basin, and potential source areas. The level of dissimilarity is based on the value of the cross-correlation coefficient. Solid black lines and dashed gray lines in the MDS plot point from each sample to its closest neighbor and second-closest neighbor, respectively. (C) Shepard plot based on 3-D MDS (stress = 0.089174).  $0.1 > \text{stress} > 0.05$  represents good degree of fitting. (D) Unmixing detrital geochronology age distributions plotted against cross-correlation coefficient. JS-ALTZ—Jinsha–Ailao tectonic zone; LCJTZ—Lancangjiang tectonic zone; M-ESPGZ—middle eastern Songpan–Ganzi complex; N-ESPGZ—north eastern Songpan–Ganzi complex; N—number of detrital zircons; NQT—North Qiangtang Block; N-YD—North Yidun Arc; S-ESPGZ—south eastern Songpan–Ganzi Complex; SQL—South Qinling tectonic zone; SQT—South Qiangtang Block; S-YD—South Yidun Arc; W-YTZ—Western Yangtze Craton.

3-D MDS plot to identify the degree of similarity of the samples. 3-D MDS was applied by constructing a pairwise dissimilarity matrix of detrital age distributions among the parent groups and daughter groups based on the  $R^2$  cross-correlation coefficient. The 3-D MDS plot and Shepard plot were generated using the program DZmids (Figs. 3B and 3C) (Saylor et al., 2018). Solid black lines and dashed gray lines in the 3-D MDS plot point from each sample to its closest neighbor and second closest neighbor, respectively.

#### Detrital Zircon U-Pb Age Unmixing Modeling

To further explore the observed variability in provenance signatures between parent groups and daughter groups, top-down detrital zircon unmixing modeling was applied to basin samples (Sundell and Saylor, 2017). Detrital zircon unmixing modeling approaches allow the potential source proportions found in a mixed basin sample to be quantified. We used the DZmix program and selected an inverse Monte Carlo approach owing to the number of potential contributing source areas (Fig. 3D) (Sundell and Saylor, 2017).

## RESULTS

### Paleocurrent Analysis

Individual paleocurrent measurements were compiled into regional and temporal trends (Fig. 2; Figs. S2 and S3). Early Cretaceous paleocurrent orientations in the northern LPB (Wengu and Fenglianchang areas) indicate SW or SSW-directed paleo-water flow, and those in the central LPB Early Cretaceous deposits (Anlongchun) indicate near-S-directed paleo-water flow. In the southeastern LPB, Early Cretaceous paleocurrent orientations from channel lag conglomerates (Mizhi, MZ01) and aqueous cross beds (Xinsheng) indicate SW-directed paleo-water flow, and large asymmetric ripples in the Nanjian area reveal a southeastward water flow. Mid-Cretaceous paleocurrent orientations

obtained from cross beds of eolian dune deposits in the northern LPB (Zhongshuifeng and Changxin, Li et al., 2018a) indicate a paleo-wind blowing toward the SW in the southeastern LPB, and mid-Cretaceous eolian deposits (Mofanghe and Xiaosanxia [XSJ]) also indicate a SW paleo-wind direction; while paleocurrents from asymmetric ripples in the Mizhi (MZ02) and the Ping An Zhuang (PAP) areas show SSW and WSW paleo-water flows, respectively. Late Cretaceous paleocurrents obtained from cross-bedded eolian dune deposits in the Yongping (Changpingtan, Zhuopanhe, and Taoyuanpu) and Yunlong (Shicheng) areas of the central LPB all indicate a SW paleo-wind direction, suggesting that the prevailing winds were located at the southern edge of the subtropical high belt or trade winds belt, which were the same as during the mid-Cretaceous (Wu et al., 2017).

### Detrital Zircon Ages from Cretaceous Rocks in the LPB

The majority of zircon grains exhibited oscillatory growth zoning in the cathodoluminescence images and had relative high Th/U ratios (Figs. S4A and S4B), indicating that most of the analyzed zircons were of igneous origin. The Lower Cretaceous (Group  $K_1JX$ ) in the southern LPB is characterized by a high density of ages at 309–202 Ma (with two peaks at ca. 224 Ma and ca. 237 Ma), 920–760 Ma (ca. 810 Ma), and 2080–1680 Ma (ca. 1840 Ma), with lesser densities at 480–420 Ma (ca. 442 Ma) and 2560–2470 Ma. The Upper Cretaceous (Group  $K_2NX$ ) in the south-central LPB shows a high density of ages at 328–200 Ma (with two peaks at ca. 225 Ma and ca. 263 Ma), 1060–720 Ma, and 2060–1640 Ma, with lesser densities at 460–360 Ma (ca. 437 Ma) and 2580–2360 Ma. The Upper Cretaceous ( $K_2HTS$ ) in the western LPB displays a high density of ages at 320–205 Ma (with a peak at ca. 232 Ma), 870–720 Ma (ca. 769 Ma), and 2070–1716 Ma, with lesser densities at 480–370 Ma (ca. 445 Ma) and 2680–2400 Ma. Results for each sample are presented in detail in Figure 3A and Figure S5.

### Variation in Detrital Zircon U-Pb Age Signatures

Detrital zircon U-Pb age signatures of samples from the LPB, SIB, and potential source areas are detailed in Figures 1 and 3A and in the Supplemental Material. In general, detrital zircon age spectra of Cretaceous samples from the LPB and SIB show marked similarities to those of the S-YD (Jian et al., 2019), as they share age subpopulations of 330–180 Ma (with a peak at ca. 261 Ma), 480–360 Ma (ca. 435 Ma), 1000–700 Ma, 2060–1710 Ma (ca. 1885 Ma), and 2610–2340 Ma (Fig. 3A), and an absence of zircon ages in the ranges of 700–500 Ma and 1700–1000 Ma (Jian et al., 2019). In addition, for the LPB, the Lower Cretaceous Group  $K_1JX$  shares a peak age at ca. 235 Ma with the LCJTZ and a peak age at ca. 443 Ma with the M-ESPGZ, indicating that the LCJTZ and M-ESPGZ might have supplied the LPB as minor source areas. The Upper Cretaceous Groups  $K_2NX$  and  $K_2HTS$  contain more zircons of age 2360–2580 Ma than Group  $K_1JX$ , similar to the N-ESPGZ. For the SIB, the Lower Cretaceous Group  $K_1SC$  shares peak ages at ca. 260 Ma and 900–700 Ma with the W-YTZ, indicating that rocks of the Late Permian Emeishan large igneous province and late Neoproterozoic bedrock in the W-YTZ probably served as potential sediment sources for the SIB (Li et al., 2018c, and references therein). The Upper Cretaceous Groups  $K_2JG$  and  $K_2GK$  share peaks at ca. 221 Ma, ca. 443 Ma, and ca. 765 Ma with the SQL, and share a peak age of ca. 1868 Ma with the S-ESPGZ, suggesting that the SQL and S-ESPGZ may have supplied clastic detritus to the SIB.

### Three-Dimensional Multidimensional Scaling Analysis

The 3-D MDS plot and Shepard plot (Figs. 3B and 3C) reveal that Cretaceous groups in the LPB and SIB display a systematic similarity to each other. All of these groups have a high correlation with the S-YD as the closest neighbor but are unrelated to the Qiangtang blocks. In addition, for the LPB, Group  $K_1JX$  has three rela-

tively closer neighbors, M-ESPGZ, JS-ALTZ, and LCJTZ, while the N-ESPGZ is considered to be the second-closest neighbor of Group  $K_2NX$ . Group  $K_2HTS$  has no obvious second-closest neighbor but has a moderate correlation with the former two groups. For the SIB, groups  $K_2JG$  and  $K_2GK$  both have the SQL as a second-closest neighbor and a moderate correlation with the S-ESPGZ.

### Unmixing Detrital Geochronology Age Distributions

The detrital zircon U-Pb age unmixing modeling results for the Cretaceous rocks of the LPB and the SIB are presented in Figure 3D, which shows Monte Carlo model source combinations plotted against the cross-correlation coefficient of the probability density plots (Sundell and Saylor, 2017). The Lower Cretaceous Jingxing Fm. (Group  $K_1JX$ ) of the LPB shows primary source contributions of 30.94% from the S-YD, 12.93% from the M-ESPGZ, 11.46% from the LCJTZ, 10.50% from the JS-ALTZ, and 34.71% from the other seven potential source areas (average contribution of 4.96%). The Upper Cretaceous Nanxing Fm. (Group  $K_2NX$ ) of the LPB shows primary source contributions of 38.97% from the S-YD, 20.15% from the N-ESPGZ, and 40.86% from the other nine potential source areas (average contribution of 4.54%). The Upper Cretaceous Hutousi Fm. (Group  $K_2HTS$ ) of the LPB shows primary source contributions of 18.06% from the S-YD, 16.39% from the N-ESPGZ, 13.72% from the M-ESPGZ, 13.48% from the SQL, and 38.35% from the other seven potential source areas (average contribution of 5.48%).

The Lower Cretaceous (Group  $K_1SC$ ) of the SIB shows primary source contributions of 44.27% from the S-YD, 15.59% from the W-YTZ, 10.43% from the S-ESPGZ, and 29.71% from the other eight potential source areas (average contribution of 3.71%; Fig. 3D). The Upper Cretaceous Jiaguan Fm. (Group  $K_2JG$ ) of the SIB shows primary source contributions of 24.25% from the S-YD, 24.11% from the S-ESPGZ, 20.63% from the SQL, and 31.00% from the other eight potential source areas (average contribution of 3.88%). The Upper Cretaceous Guankou Fm. (Group  $K_2GK$ ) of the SIB shows primary source contributions of 23.91% from the S-YD, 25.33% from the SQL, 12.51% from the S-ESPGZ, and 38.24% from the other eight potential source areas (average contribution of 4.78%). Overall, the detrital zircon U-Pb age unmixing modeling results were highly consistent with those of the 3-D MDS, with the former analysis providing a more detailed and comprehensive account of the proportions of provenance contribution.

## DISCUSSION

### High-Altitude Late Mesozoic Terrain in the SE Tibetan Plateau and Drainage Network Evolution

Basins along the SE Tibetan Plateau area experienced a marked shift in paleoclimate during the Cretaceous. During the Early Cretaceous, almost all these basins were characterized by alluvial-fluvial-lacustrine deposits and paleosols (Fig. S1) (Wu et al., 2017; Li et al., 2018a, 2018c; Liu et al., 2019; Wang et al., 2021, 2023), indicating that the climate was semi-humid to semi-arid. By the mid- to Late Cretaceous, the climate had become increasingly hot and arid, leading to a gradual shift from aqueous systems to eolian systems (Wu et al., 2022). These interpretations are supported by Upper Cretaceous eolian sands and evaporites found in all these basins (Wu et al., 2017, 2022; Li et al., 2018a, 2018c; Liu et al., 2019; Wang et al., 2021, 2023). This pronounced and coeval climatic shift over the SE Tibetan Plateau was previously thought to have been controlled by latitudinal migration of subtropical high-pressure systems on a planetary scale (Wu et al., 2017; Li et al., 2018a), which is consistent with our paleo-wind orientations reconstruction (Figs. 2, 4A, and 4E). However, these basins were adjacent to the Neo-Tethys (Fig. 4), and moisture would have extended to the continental interiors, given the differences in ocean-continental thermodynamic properties and meridional heat transport by the atmosphere and/or oceans during the Cretaceous greenhouse world (Fluteau et al., 2007; Wu et al., 2017). Warm ocean currents circulating in the Neo-Tethys (Fig. 4) (Scotese, 2002) would have also humidified these areas and thus probably slowed aridification in east Asia. In contrast, there was intensive aridification in the interior of the SE Tibetan Plateau during the mid- to Late Cretaceous (Wu et al., 2017; Li et al., 2018a, 2018c). Generally, the interaction between features such as high-pressure systems, high mountains, and cold ocean currents determines whether a given region will undergo desertification (Glennie, 1970; Cook, 1993; Wu et al., 2017). Therefore, it is likely that the paleoclimate and erg system of the SE Tibetan Plateau area during the Cretaceous was controlled by a large and relatively enclosed paleo-topographic barrier that triggered a rain-shadow effect and dominated the evolution of the sediment-routing system before the India-Eurasia collision.

For the Early Cretaceous (Barremian–Hauterivian), detrital zircon age spectra signatures of groups  $K_1JX$  from the Lanping Basin (LPB) and  $K_1SC$  from the Sichuan Basin (SIB) show pronounced similarities with that of the

South Yidun Arc (S-YD), suggesting that the S-YD was the main source area and a prominent upland in the SE Tibetan Plateau during this epoch (Figs. 3A and 4A). Regional low temperature thermochronology data and corresponding thermal history modeling of the Zhongza, Ganzi, and Daocheng granitoids from the Yidun Arc (Reid et al., 2005; Wilson and Fowler, 2011; Tian et al., 2014a; Leng et al., 2018), show that rapid cooling episodes between Late Jurassic to Late Cretaceous occurred in the S-YD (Fig. 5). This indicates a regional uplift during the period, probably as a result of the northward subduction of the Meso-Tethys oceanic slab and subsequent collision between the Lhasa and Qiangtang terranes (Tian et al., 2014a). Furthermore, 206–138 Ma syn-collision granites are widely exposed in the Yidun Arc, which also suggests that this area was located in an arc-continent collision setting (Hou et al., 2001). Therefore, the drainage systems from the S-YD to the LPB and the SIB can be estimated (Figs. 4A and 4B). Early Cretaceous paleocurrent orientations from fluvial deposits in the northern LPB are SW or SSW to SE (Fig. 2), and in the southern LPB the drainage routes connect with channels developed in the central Simao Basin (Wu et al., 2017), and may even extend to the Muang Xai Basin in Laos (Wang et al., 2017), the Khorat Basin in Thailand, and the Phuquoc Basin in the Gulf of Thailand (Nguyen et al., 2021; Wang et al., 2021, 2023).

Results of 3-D MDS and DZ unmixing modeling show that the primary provenance area for Group  $K_1JX$  is the S-YD, with minor contributions from the Lancangjiang tectonic zones (LCJTZ) and middle depocenter of eastern Songpan–Ganzi Complex (M-ESPGZ), whereas Group  $K_1SC$  shows primary contributions by the S-YD and minor contributions by the Western Yangtze (W-YTZ) and southern depocenter of eastern Songpan–Ganzi Complex (S-ESPGZ) (Figs. 3A–3D). The LCJTZ provided ca. 235 Ma zircons from proximal intrusive rocks to the LPB (Fig. 3A), and the M-ESPGZ contributed a small amount of detrital material to the LPB, which may represent the inheritance of orogenesis in the eastern Songpan–Ganzi during the Late Triassic (Weislogel et al., 2010). The minor contributions of the W-YTZ and S-ESPGZ to Group  $K_1SC$  may represent detrital materials carried by the drainage system from the S-YD to the SIB through the W-YTZ and S-ESPGZ (Figs. 4A and 4B). It should be noted that during the development of the drainage system from the S-YD to the LPB and SIB, if materials sourced from the M-ESPGZ were transported to the LPB, then another drainage system would have developed simultaneously to the west of that drainage system (Fig. 4B), as suggested by a previous paleo-

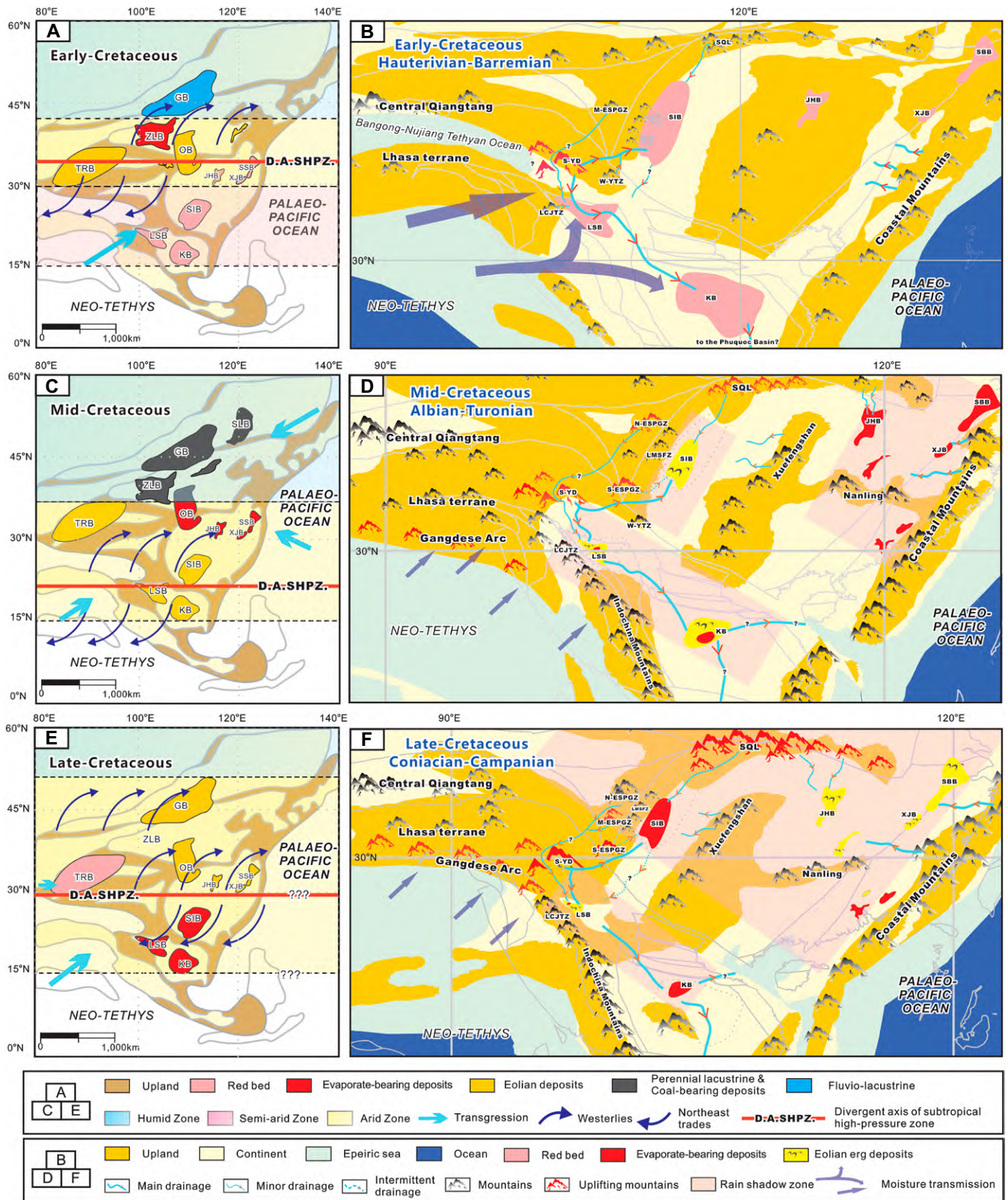


**Figure 4. Spatial-temporal variation in the distribution of climate-indicative sediments in the Asian interior (Wu et al., 2018), drainage evolution (Wu et al., 2017; Suo et al., 2019; Nguyen et al., 2021; Zhao et al., 2021; Wang et al., 2021, 2023), and paleogeography of the SE Tibetan Plateau (Metcalf, 2011; Cao et al., 2017) during the Early (A and B), mid- (C and D), and Late (E and F) Cretaceous. GB—Gobi Basin; JHB—Jiangnan Basin; KB—Khorat Basin; LSB—Lanping-Simao Basin; OB—Ordos Basin; SBB—Subei Basin; SIB—Sichuan Basin; SLB—Songliao Basin; XJB—Xinjiang Basin; ZLB—Zoulang Basin.**

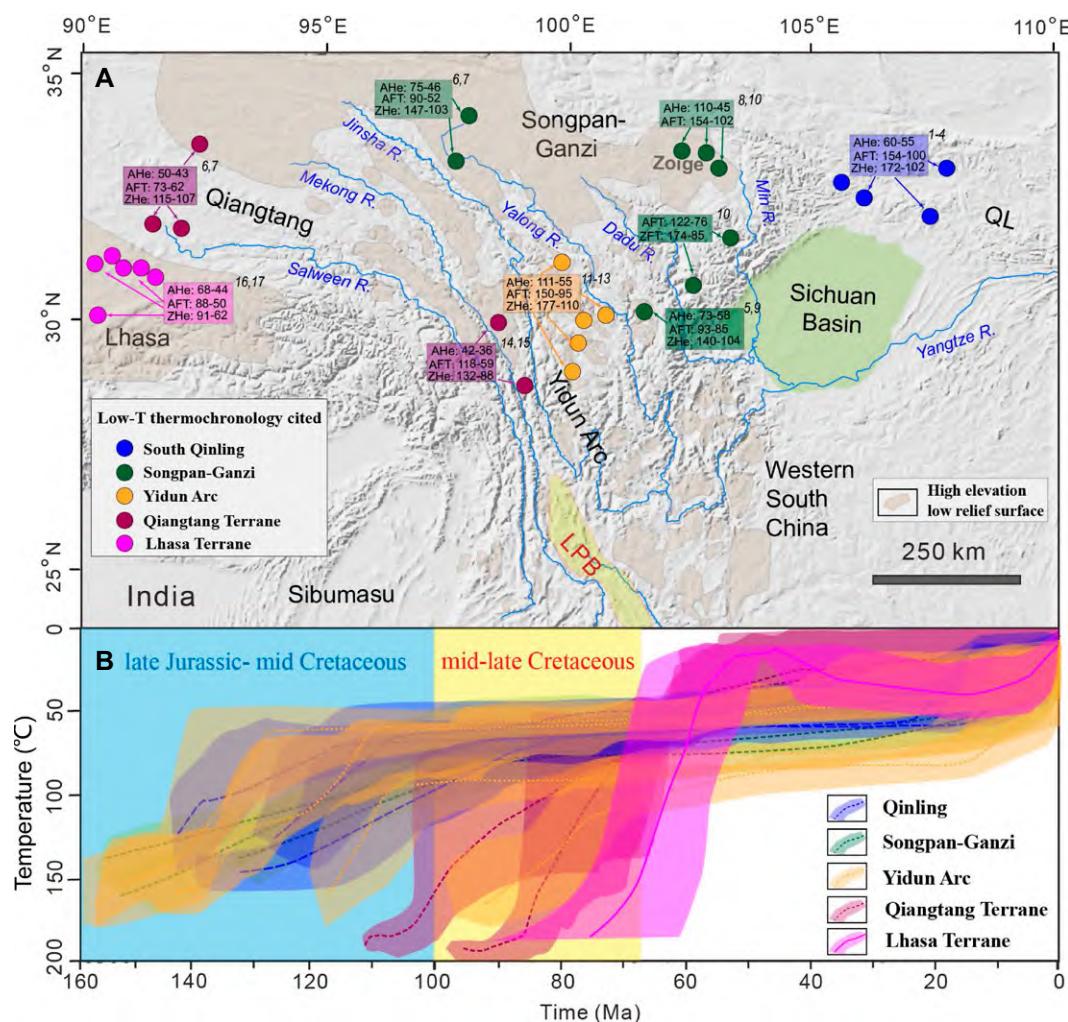


**Figure 5.** (A) The distribution of modern topography, drainage system in eastern Tibet and surrounding areas, along with locations of low-temperature (T) thermochronology samples from the plateau surface. The highlighted areas in gray represent low relief, high elevation areas, cited from Clark et al. (2005). (B) Thermal modeling results of these thermochronological data from previous studies. The thermal modeling results cited from previous studies show that the mid- to Late Cretaceous cooling/exhumation episodes in the Qinling area (1—Chen et al., 2015; 2—Enkelmann et al., 2006; 3—Wang et al., 2021; 4—Tian et al., 2012) and eastern Songpan-Ganzi complex (5—Clark et al., 2005; 6—Wang et al., 2008; 7—Dai et al., 2013; 8—Tian et al., 2014b; 9—Zhang et al., 2016; 10—Li et al., 2023), and the Late Jurassic to mid-Cretaceous rapid cooling episodes occurred in the South Yidun Arc (11—Wilson and Fowler, 2011; 12—Tian et al., 2014a; 13—Leng et al., 2018), and in the mid-Cretaceous to Paleocene in the Qiangtang Terrane (14–15—Cao et al.,

2021, 2022), and in the Late Cretaceous to Paleocene in the Lhasa Terrane (16—Hetzl et al., 2011; 17—Haider et al., 2013). AFT—apatite fission track dating; AHe—apatite (U-Th)/He dating; LPB—Lanping Basin; R.—River; ZHe—zircon (U-Th)/He dating.

geographic study (BGMRYP, 1995). Regarding the connectivity between the LPB and SIB, previous studies hold that the paleo-Yangtze River coursed through the SIB, Xichang Basin, and LPB from the Middle Jurassic to Early Cretaceous (Chen, 1979). The southwestward paleo-water flow and thick Early Cretaceous fluvial lag deposits cropping out in the Mizhi area of the southeastern LPB (Fig. 2; Fig. S2) suggest long-distance transport of detrital material from the northeastern source area (Fig. 4B). Consequently, we do not rule out the possibility that the LPB was connected to the SIB during the Early Cretaceous and that the Mizhi-Nanjiang area may have been an important river confluence in east Asia at that time.

For the mid-Cretaceous (Albian–Turonian), detrital zircon age spectra signatures of groups  $K_2NX$  and  $K_2JG$  show inheritance of Early Cretaceous sediments (Figs. 4C and 4D), suggesting

that the S-YD was still the dominant source area for the LPB and SIB at that time, with a pulse of moderate to high exhumation (70–300 m/m.y.) (Liu-Zeng et al., 2018), and that the main drainage systems were still active (Figs. 4C and 4D). In addition, the northern depocenter of the eastern Songpan-Ganzi Complex (N-ESPGZ) accounted for 20.15% of the provenance contribution to the LPB during the mid-Cretaceous (Fig. 3D), 13.97% more than during the Early Cretaceous, suggesting the occurrence of local uplift and the establishment of a new source area in the N-ESPGZ. This tectonic information is confirmed by multiple low-temperature thermochronological data and thermal history modeling results (Xu et al., 2016; Liu et al., 2019) (Fig. 5), together pointing to a rapid mid-Cretaceous cooling/exhumation event (ca. 100 Ma) in the Zoige and surrounding areas (Tian et al., 2014b; Liu et al., 2019) (Fig. 5). Meanwhile, owing to

the compression of the Qinling orogen toward the Yangtze Craton the compression caused rapid uplift and denudation in the northern SIB (Fig. 5) (Li et al., 2018c). Moreover, the marked mid-Cretaceous (ca. 100–80 Ma) cooling of granitoids in the Litang-Yajiang area indicates that the S-ESPGZ had also become a new source area for the SIB (Fig. 5) (Wilson and Fowler, 2011). These two source areas (the South Qinling tectonic zones [SQL] and the S-ESPGZ) of the SIB are confirmed by the results of 3-D MDS and DZ unmixing modeling (Figs. 3B–3D), with these two source areas estimated to have contributed 24.11% and 20.63%, respectively, of the detrital materials to the SIB, therefore, being minor sources areas during the mid-Cretaceous. As the marked surface uplift of the SE Tibetan Plateau and the resultant climate had transitioned to one characterized by extreme aridity during the mid-Cretaceous, eolian sands and evapo-

rites became widely developed in the LPB and SIB (Fig. 4D), with drainage systems being less developed than those of the Early Cretaceous, and deserts and shallow playa were initially formed (Wu et al., 2017; Li et al., 2018a, 2018c; Wang et al., 2021, 2023), even resulting in ice flow formation and dropstone accumulations in desert oases (Wu and Rodríguez-López, 2021). Both the LPB and SIB began to shrink dramatically during the mid-Cretaceous, with many fluvial channels within basins being abandoned in favor of wadis (Li et al., 2018a), and connectivity between the LPB and SIB was lost (Chen, 1979). However, we consider that the main drainage systems from the S-YD and the northern depocenter of eastern Songpan–Ganzi Complex to the LPB, and from the S-YD and the southern depocenter of the eastern Songpan–Ganzi Complex to the SIB, were active on the basis of the southwestward paleo-water flow in the MFH, XSJ, and MZ02 areas of LPB (Fig. 2) and detrital zircon age spectra signatures (Fig. 3).

Detrital zircon age spectra signatures of groups  $K_2$ -HTS and  $K_2$ -GK show that although the S-YD continued to provide detrital materials for the LPB and the SIB during the Late Cretaceous (Coniacian–Campanian), its contribution was no longer dominant. For the LPB, the contribution from the Songpan–Ganzi (N-ESPGZ and M-ESPGZ, 30.11%) exceeded that of the S-YD (18.60%), whereas for the SIB, the contribution of the SQL (25.34%) was similar to that of the S-YD (23.91%), all of which can be attributed to continuous uplift of the Songpan–Ganzi Complex and the South Qinling orogen from the mid-Cretaceous (Xu et al., 2016; Liu et al., 2019). This is consistent with widespread Cretaceous cooling ages reported from the high altitude and low relief surfaces in the Songpan–Ganzi terrane (Clark et al., 2005; Dai et al., 2013; Tian et al., 2014a, 2014b; Cao et al., 2021), as well as the west Qinling orogen (Chen et al., 2015; Enkelmann et al., 2006; Wang, 2021; Tian et al., 2012), probably related to the Lhasa–Qiangtang collision (the closure process of the Bangong–Nujiang Tethyan Ocean, Kapp and Decelles, 2019; Han et al., 2021; Lai et al., 2019a; Luo et al., 2022). Thermal modeling results for these high altitude and low relief surfaces in the region generally show an Early Cretaceous rapid cooling episode, followed by a quiet slow cooling scenario from Late Cretaceous to late Cenozoic (Fig. 5). The long-term slow cooling probably indicates that a flat surface formed. Hence, combined with a series of structural and sedimentological evidence and thickening crust, the eastern Songpan–Ganzi terrane had formed a high elevation and low relief surface (paleo-plateau) in the Late Cretaceous (Liu et al., 2019). In addition, the boundary fault zones within the Songpan–

Ganzi (Tian et al., 2014b; Li et al., 2023) and Qinling orogen (especially its west and south parts, Chen et al., 2015; Wang et al., 2021; Tian et al., 2012) also show some Late Cretaceous cooling ages and a Late Cretaceous rapid cooling/exhumation episode (Fig. 5B) suggesting a sustained uplifted topography in the region.

Along with the expanding of the high-altitude terrain in the SE Tibetan Plateau area during the Late Cretaceous, intermontane basins in the South China Block and Indochina Block became increasingly enclosed (Fig. 4F). The LPB was still dominated by eolian sands, whereas the SIB underwent deposition of evaporites, and the hot and dry climate persisted in both of these two basins and more widely throughout east Asia during the Late Cretaceous (Figs. 4E and 4F) (Wu et al., 2018, 2022). We consider that the pattern of drainage systems during the Late Cretaceous was similar to that of the mid-Cretaceous, except that the SQL provided more clastic materials to the SIB, the LPB and SIB may have been reconnected, and the desertification center of the LPB migrated into the basin interior (Figs. 4E and 4F). Given the mid- to Late Cretaceous paleotopography of east Asia, which was high in the east and west and low in the south (Figs. 4C–4F), and given the increased detrital contribution from the SQL to Late Cretaceous sediments of the LPB compared with the mid-Cretaceous, we estimate that the major drainage routes were southward during the Late Cretaceous and might have been directed along the line connecting the SIB to the Lanping–Simao Basin to the Phuquoc Basin (Figs. 4C–4F). The region to the south of the Phuquoc Basin may have been one of the estuaries for the detrital material transportation from the east Asian continent during the mid- to Late Cretaceous. This hypothesis is supported by recent reconstructions of the Cretaceous regional drainage system (Wang et al., 2021; Nguyen et al., 2021; Zhao et al., 2021).

### Cretaceous Mountain System and Rain Shadows in East Asia

Our reconstruction of paleotopography and drainage systems (Fig. 4) shows that from the mid-Cretaceous, the SE Tibetan Plateau initially formed a growing north-south oriented barrier consisting of the Gangdese–Lhasa–Qiangtang–Yidun–Songpan–Ganzi–Lancang–Lincang–Western Indochina areas (Figs. 4C–4F). The windward side of the barrier, including the Lhasa and South Qiangtang blocks, was dominated by deposition of marine sediment during the Early Cretaceous, followed by deposition of terrestrial molasse (alluvial or braided fluvial facies) through to the mid-Cretaceous, indicating a relatively humid environment (Liu et al., 2019). The

Neo-Tethys oceanic plate and the Asian continental plate converged during the Cretaceous, resulting in Cordilleran/Andean-style magmatic activity (Gangdese arc) and mountain building in the southern Tibetan Plateau (Tapponnier, et al., 1981; Burg and Chen, 1984; Ding et al., 2022; Wu et al., 2022). Based on sedimentological and provenance analysis, Lai et al. (2019b) proposed that the north Lhasa terrane (named as Northern Lhasaplano) had started uplifting since ca. 92 Ma. In contrast, on the leeward side of the barrier during the same time interval, sedimentation in basins of the continental interior underwent a shift from fluvial-lacustrine red-beds with paleosols to extensive erg systems (Wu et al., 2017, 2022; Li et al., 2018a, 2018c), indicating a dry or extremely dry climate leaving a thick record of eolian activity in these basins. All these interpretations suggest that the topographic barrier acted as a drainage divide, with the leeward side forming a vast rain-shadow area spanning the western South China Block and Indochina Block (Figs. 4A–4D). By the Late Cretaceous, the process of aridification in the east Asia interior was also influenced by the superposition of coastal mountains or plateaus along the eastern margin of Asia (Wu et al., 2018; Suo et al., 2019), causing the interior of the continent to become even more enclosed, and deserts and playas became widely developed in intermontane basins (Wu et al., 2022) as the rain shadow expanded to the whole east Asian continent (Figs. 4E and 4F).

The above-described rain-shadow effect of east Asia during the Cretaceous was partly similar to that of a linear mountain range like the Andes (Rech et al., 2019) but closer to the aridification pattern of the Asian interior caused by Cenozoic uplift of the Tibetan Plateau (Dupont-Nivet et al., 2007). Evidence for the large-scale rain-shadow effect, combined with the paleo-configuration of the coastal mountains, Qiangtang, Lhasa, and Gangdese mountain ranges (Fig. 4, Wu et al., 2018; Suo et al., 2019; Kapp and Decelles, 2019; Ding et al., 2022), suggests that a complex of mountain systems or even plateau landform developed in the margin and hinterland of Asia during the mid- to Late Cretaceous, and thus, we consider these landforms collectively as the early growth of the Tibetan Plateau with the predominant tendency of their drainage systems to flow from west and east to the south (Fig. 4). This enclosed pattern of landforms in east Asia had a profound influence on the paleoclimate of this region, whether within the westerlies or subtropical-high pressure belt (Figs. 4D and 4F), whereby moisture could not be effectively transported to the interior, giving rise to aridification and even desertification. The present study challenges the previous view that the Late Cretaceous paleotopography of east

Asia was high in the east and low in the west, with the tendency of drainage systems to flow from east to west (Wang, 1998), and instead proposes that east Asia was high in both the east and west, or even an enclosed continent composed of a series of highlands during this interval (Fig. 4F).

## CONCLUSIONS

Our integrated study based on data from paleocurrents, detrital zircon U-Pb geochronology, tectonic-magmatic activity, and low-temperature thermochronology allows us to propose a model of the spatial and temporal variation in surface uplift and drainage system configuration for the SE Tibetan Plateau throughout the Cretaceous. Our results suggest that tectonically induced surface uplift of the SE Tibetan Plateau area (particularly the South Yidun Arc–eastern Songpan Garze area), combined with the mountain building in southern Tibetan Plateau (Gangdese arc), occurred during the mid- to Late Cretaceous, resulting in the formation of an extensive topographic barrier and subcontinental-scale rain-shadow effect, which led to widespread aridification spanning the South China and Indochina blocks and a reorganization of regional drainage systems. In addition, with superimposition by coastal mountains or plateaus in the eastern margin of Asia, east Asia during the mid- to Late Cretaceous was characterized by a landscape that was high in both the east and west, with drainage systems tending to flow from the west and east to the south. This topographic configuration is in marked contrast to that proposed previously, whereby topography was high in the east and low in the west and drainage accordingly flowing from east to west. Our results for the Cretaceous topography and drainage of east Asia have implications for re-examining the models of Cenozoic tectonics of the Tibetan Plateau, atmospheric circulation patterns, the origin of the Asian monsoon system, intracontinental aridification, and the evolution of the modern drainage system in east Asia.

## ACKNOWLEDGMENTS

We thank Gaojie Li, Tao Yuan, Yun Chen, Zheng Gong, Yu Hou, and Hailei Tang for their assistance in the field and helpful discussion. This work was jointly funded by the National Natural Science Foundation of China (41872099, 42230310, 91855213, 41602127), Natural Science Foundation of Hunan Province of China (2021JJ30388), and Open Foundation of Hubei Key Laboratory of Paleontology and Geological Environment Evolution (Wuhan Center of China Geological Survey, PEL-202203). This work is also funded by the “Convocatoria de Ayudas para la recalificación del sistema universitario Español 2021-2023, Financiado por la Unión Europea-Next

Generation EU.” Vicerrectorado de Investigación, Universidad del País Vasco, UPV/EHU to Juan Pedro Rodríguez-López. This work is a contribution to the Research Group of the Basque Government IT-1602-22 (Grupo Consolidado del Gobierno Vasco IT-1602-22).

## REFERENCES CITED

- Bally, A.W., Allen, C.R., Geyer, R.B., Hamilton, W.B., Hopson, C.A., Molnar, P.H., Oliver, J.E., Opdyke, N.D., Pfaffner, G., and Wu, F.T., 1980, Notes on the geology of Tibet and adjacent areas; report of the American plate tectonics delegation to the People's Republic of China: U.S. Geological Survey Open-File Report 80-501, 100 p., <https://doi.org/10.3133/ofr80501>.
- BGMRYP (Bureau of Geology and Mineral Resources of Yunnan Province), 1995, Atlas of the Sedimentary Facies and Paleogeography of Yunnan: Kunming, China, Yunnan Science and Technology Press, 228 p. [in Chinese with English abstract].
- Bosboom, R., Dupont-Nivet, G., Grothe, A., Brinkhuis, H., Villa, G., Mandic, O., Stoica, M., Huang, W., Yang, W., Guo, Z., and Krijgsman, W., 2014, Linking Tarim Basin sea retreat (west China) and Asian aridification in the late Eocene: *Basin Research*, v. 26, no. 5, p. 621–640, <https://doi.org/10.1111/bre.12054>.
- Burchfiel, B.C., and Chen, Z., 2013, Tectonics of the Southeastern Tibetan Plateau and its Adjacent Foreland: *Geological Society of America Memoir* 210, 164 p., <https://doi.org/10.1130/MEM210>.
- Burg, J.P., and Chen, G.M., 1984, Tectonics and structural zonation of southern Tibet, China: *Nature*, v. 311, p. 219–223, <https://doi.org/10.1038/311219a0>.
- Cao, K., Hervé Leloup, P., Wang, G., Liu, W., Mahéo, G., Shen, T., Xu, Y., Sorrel, P., and Zhang, K., 2021, Thrusting, exhumation, and basin fill on the western margin of the South China block during the India-Asia collision: *Geological Society of America Bulletin*, v. 133, p. 74–90, <https://doi.org/10.1130/B35349.1>.
- Cao, K., Tian, Y., van der Beek, P., Wang, G., Shen, T., Reiners, P., Bernet, M., and Husson, L., 2022, Southwestward growth of plateau surfaces in eastern Tibet: *Earth-Science Reviews*, v. 232, <https://doi.org/10.1016/j.earscirev.2022.104160>.
- Cao, S., Zhang, L., Wang, C., Ma, J., Tan, J., and Zhang, Z., 2020, Sedimentological characteristics and aeolian architecture of a plausible intermountain erg system in Southeast China during the Late Cretaceous: *Geological Society of America Bulletin*, v. 132, p. 2475–2488, <https://doi.org/10.1130/B35494.1>.
- Cao, W., Zahirovic, S., Flament, N., Williams, S., Golonka, J., and Müller, R.D., 2017, Improving global paleogeography since the late Paleozoic using paleobiology: *Biogeosciences*, v. 14, p. 5425–5439, <https://doi.org/10.5194/bg-14-5425-2017>.
- Carrapa, B., DeCelles, P.G., Wang, X., Clementz, M.T., Mancin, N., Stoica, M., Kraatz, B., Meng, J., Abdulov, S., and Chen, F., 2015, Tectono-climatic implications of Eocene Paratethys regression in the Tajik basin of central Asia: *Earth and Planetary Science Letters*, v. 424, p. 168–178, <https://doi.org/10.1016/j.epsl.2015.05.034>.
- Chen, H., Hu, J., Wu, G., Shi, W., Geng, Y., and Qu, H., 2015, Apatite fission-track thermochronological constraints on the pattern of late Mesozoic–Cenozoic uplift and exhumation of the Qinling Orogen, central China: *Journal of Asian Earth Sciences*, v. 114, p. 649–673, <https://doi.org/10.1016/j.jseas.2014.10.004>.
- Chen, K., 2017, Provenance Analysis of the Late Cretaceous Yunlong Formation in the Lanping Basin, Yunnan Province and its tectonic implications [Master dissertation]: Beijing, China, China University of Geosciences, 84 p. [in Chinese with English abstract].
- Chen, K., Gao, S., Wu, Y.B., Guo, J.L., Hu, Z.C., Liu, Y.S., Zong, K.Q., Liang, Z.W., and Geng, X.L., 2013, 2.6–2.7 Ga crustal growth in Yangtze craton, South China: *Precambrian Research*, v. 224, p. 472–490, <https://doi.org/10.1016/j.precamres.2012.10.017>.
- Chen, P.J., 1979, An outline of paleogeography during the Jurassic and Cretaceous periods of China: With

a discussion on the origin of Yangtze River: *Acta Scientiarum Naturalium Universitatis Pekinesis*, v. 3, p. 90–109.

- Chen, P.J., 2000, Paleoenvironmental changes during the Cretaceous in eastern China, in Hakuyu, O., and Nlall, J.M., eds., *Cretaceous Environments of Asia: Developments in Palaeontology and Stratigraphy*: Amsterdam, Netherlands, Elsevier, v. 17, p. 81–90, [https://doi.org/10.1016/S0920-5446\(00\)80025-4](https://doi.org/10.1016/S0920-5446(00)80025-4).
- Chen, Q., Sun, M., Long, X.P., Zhao, G.C., Wang, J., Yu, Y., and Yuan, C., 2018, Provenance study for the Paleozoic sedimentary rocks from the West Yangtze Block: Constraint on possible link of South China to the Gondwana supercontinent reconstruction: *Precambrian Research*, v. 309, p. 271–289, <https://doi.org/10.1016/j.precamres.2017.01.022>.
- Chen, Y., Yan, M., Fang, X., Song, C., Zhang, W., Zan, J., Zhang, Z., Li, B., Yang, Y., and Zhang, D., 2017, Detrital zircon U-Pb geochronological and sedimentological study of the Simao Basin, Yunnan: Implications for the Early Cenozoic evolution of the Red River: *Earth and Planetary Science Letters*, v. 476, p. 22–33, <https://doi.org/10.1016/j.epsl.2017.07.025>.
- Clark, M.K., Schoenbohm, L.M., Royden, L.H., Whipple, K.X., Burchfiel, B.C., Zhang, X., Tang, W., Wang, E., and Chen, L., 2004, Surface uplift, tectonics, and erosion of eastern Tibet from large-scale drainage patterns: *Tectonics*, v. 23, no. 1, <https://doi.org/10.1029/2002TC001402>.
- Clark, M.K., House, M.K., Royden, L.H., Whipple, K.H., Burchfiel, B.C., Zhang, X., and Tang, W., 2005, Late Cenozoic uplift of southeastern Tibet: *Geology*, v. 33, p. 525–528, <https://doi.org/10.1130/G21265.1>.
- Cook, A.A., 1993, Handcuff neuropathy among U.S. prisoners of war from Operation Desert Storm: *Military Medicine*, v. 158, p. 253–254, <https://doi.org/10.1093/milmed/158.4.253>.
- Dai, J.G., Wang, C.S., Hourigan, J., and Santosh, M., 2013, Insights into the early Tibetan Plateau from (U-Th)/He thermochronology: *Journal of the Geological Society*, v. 170, p. 917–927, <https://doi.org/10.1144/jgs2012-076>.
- Dewey, J.F., Shackleton, R.M., Chengfa, C., and Yiyin, S., 1988, The tectonic evolution of the Tibetan Plateau: *Philosophical Transactions of the Royal Society A: Mathematical, Physical and Engineering Sciences*, v. 327, no. 1594, p. 379–413, <https://doi.org/10.1098/rsta.1988.0135>.
- Ding, L., Kapp, P., Cai, F., Garzzone, C.N., Xiong, Z., Wang, H., and Wang, C., 2022, Timing and mechanisms of Tibetan Plateau uplift: *Nature Reviews: Earth & Environment*, v. 3, p. 652–667, <https://doi.org/10.1038/s43017-022-00318-4>.
- Dong, Y.P., Liu, X.M., Neubauer, F., Zhang, G.W., Tao, N., and Zhang, Y.G., 2013, Timing of Paleozoic amalgamation between the North China and South China blocks: Evidence from detrital zircon U-Pb ages: *Tectonophysics*, v. 586, p. 173–191, <https://doi.org/10.1016/j.tecto.2012.11.018>.
- Duan, L., Meng, Q.R., Zhang, C.L., and Liu, X.M., 2011, Tracing the position of the South China Block in Gondwana: U-Pb ages and Hf isotopes of Devonian detrital zircons: *Gondwana Research*, v. 19, p. 141–149, <https://doi.org/10.1016/j.gr.2010.05.005>.
- Dupont-Nivet, G., Krijgsman, W., Langereis, C.G., Abels, H.A., Dai, S., and Fang, X., 2007, Tibetan plateau aridification linked to global cooling at the Eocene-Oligocene transition: *Nature*, v. 445, p. 635–638, <https://doi.org/10.1038/nature05516>.
- England, P.C., and Houseman, G.A., 1988, The mechanics of the Tibetan Plateau: *Philosophical Transactions of the Royal Society A: Mathematical, Physical and Engineering Sciences*, v. 326, p. 301–320, <https://doi.org/10.1098/rsta.1988.0089>.
- Enkelmann, E., Ratschbacher, L., Jonckheere, R., Nestler, R., Fleischer, M., Gloaguen, R., Hacker, B.R., Yue, Q.Z., and Ma, Y.S., 2006, Cenozoic exhumation and deformation of northeastern Tibet and the Qinling: Is Tibetan lower crustal flow diverging around the Sichuan Basin: *Geological Society of America Bulletin*, v. 118, p. 651–671, <https://doi.org/10.1130/B25805.1>.

- Farnsworth, A., Lunt, D.J., Robinson, S.A., Valdes, P.J., Roberts, W.H.G., Clift, P.D., Markwick, P., Su, T., Wrobel, N., Bragg, F., Kelland, S.-J., and Pancost, R.D., 2019, Past East Asian monsoon evolution controlled by paleogeography, not CO<sub>2</sub>: *Science Advances*, v. 5, no. 10, <https://doi.org/10.1126/sciadv.aax1697>.
- Fluteau, F., Ramstein, G., Besse, J., Guiraud, R., and Masse, J.P., 2007, Impacts of palaeogeography and sea level changes on Mid-Cretaceous climate: *Palaeogeography, Palaeoclimatology, Palaeoecology*, v. 247, p. 357–381, <https://doi.org/10.1016/j.palaeo.2006.11.016>.
- Gehrels, G., Kapp, P., Decelles, P., Pullen, A., Blakey, R., Weislogel, A., Ding, L., Gwynn, J., Martin, A., McQuarrie, N., and Yin, A., 2011, Detrital zircon geochronology of pre-Tertiary strata in the Tibetan-Himalayan orogen: *Tectonics*, v. 30, p. 1–27, <https://doi.org/10.1029/2011TC002868>.
- Glennie, K.W., 1970, *Desert Sedimentary Environments*: New York, USA, Elsevier, 222 p.
- Guo, Z.T., Ruddiman, W.F., Hao, Q.Z., Wu, H.B., Qiao, Y.S., Zhu, R.X., Peng, S.Z., Wei, J.J., Yuan, B.Y., and Liu, T.S., 2002, Onset of Asian desertification by 22 Myr ago inferred from loess deposits in China: *Nature*, v. 416, p. 159–163, <https://doi.org/10.1038/416159a>.
- Haider, V., Dunkl, I., von Eynatten, H., Ding, L., Frei, D., and Zhang, L.Y., 2013, Cretaceous to Cenozoic evolution of the northern Lhasa Terrane and the early Paleogene development of peneplains at Nam Co, Tibetan Plateau: *Journal of Asian Earth Sciences*, v. 70–71, p. 79–98, <https://doi.org/10.1016/j.jseas.2013.03.005>.
- Han, X., Dai, J.G., Lin, J., Xu, S.Y., Liu, B.R., Wang, Y.N., and Wang, C.S., 2021, The middle cretaceous (110–94 Ma) evolution of Tangza Basin in the western Tibetan Plateau and implications for initial topographic growth of northern Lhasa: *Geological Society of America Bulletin*, v. 133, p. 1283–1300, <https://doi.org/10.1130/B35708.1>.
- Harrowfield, M.J., and Wilson, C.J.L., 2005, Indosinian deformation of the Songpan Garzê Fold Belt, northeast Tibetan Plateau: *Journal of Structural Geology*, v. 27, p. 101–117, <https://doi.org/10.1016/j.jsg.2004.06.010>.
- He, D.F., Zhu, W.G., Zhong, H., Ren, T., Bai, Z.J., and Fan, H.P., 2013, Zircon U-Pb geochronology and elemental and Sr-Nd-Hf isotopic geochemistry of the Daocheng granitic pluton from the Yidun Arc, SW China: *Journal of Asian Earth Sciences*, v. 67–68, p. 1–17, <https://doi.org/10.1016/j.jseas.2013.02.002>.
- Hetzl, R., Dunkl, I., Haider, V., Strobl, M., von Eynatten, H., Ding, L., and Frei, D., 2011, Peneplain formation in southern Tibet predates the India-Asia collision and plateau uplift: *Geology*, v. 39, p. 983–986, <https://doi.org/10.1130/G32069.1>.
- Hou, Z., Qu, X., Zhou, J., Yang, Y., Huang, D., Lv, Q., Tang, S., Yu, J., Wang, H., and Zhao, J., 2001, Collision-orogenic processes of the Yidun Arc in the Sanjiang Region: Record of granites: *Acta Geologica Sinica*, v. 75, p. 484–497 [in Chinese with English abstract].
- Jian, X., Weislogel, A.L., and Pullen, A., 2019, Triassic sedimentary filling and closure of the eastern Paleo-Tethys Ocean: New insights from detrital zircon geochronology of Songpan-Ganzi, Yidun, and West Qinling flysch in eastern Tibet: *Tectonics*, v. 38, p. 767–787, <https://doi.org/10.1029/2018TC005300>.
- Kapp, P.A., and Decelles, P.G., 2019, Mesozoic–Cenozoic geological evolution of the Himalayan-Tibetan orogen and working tectonic hypotheses: *American Journal of Science*, v. 319, p. 159–254, <https://doi.org/10.2475/03.2019.01>.
- Lai, W., Hu, X., Garzanti, E., Xu, Y., Ma, A., and Li, W., 2019a, Early cretaceous sedimentary evolution of the northern Lhasa terrane and the timing of initial Lhasa-Qiangtang collision: *Gondwana Research*, v. 73, p. 136–152, <https://doi.org/10.1016/j.gr.2019.03.016>.
- Lai, W., Hu, X., Garzanti, E., Sun, G., Garzzone, C.N., Boudagher-Fadel, M., and Ma, A., 2019b, Initial growth of the northern Lhasaplano, Tibetan Plateau in the early Late Cretaceous (ca. 92 Ma): *Geological Society of America Bulletin*, v. 131, no. 11–12, p. 1823–1836, <https://doi.org/10.1130/B35124.1>.
- Leng, C.B., Cooke, D.R., Hou, Z.-Q., Evans, N.J., Zhang, X.-C., Chen, W.T., Danišik, M., McInnes, B.I.A., and Yang, J.-H., 2018, Quantifying exhumation at the giant Pulang porphyry Cu-Au deposit using U-Pb-He dating: *Economic Geology*, v. 113, p. 1077–1092, <https://doi.org/10.5382/econgeo.2018.4582>.
- Li, G.J., Wu, C.H., Rodríguez-López, J.P., Yi, H.S., Xia, G.Q., and Wagreich, M., 2018a, Mid-Cretaceous aeolian desert systems in the Yunlong area of the Lanping Basin, China: Implications for palaeoatmosphere dynamics and paleoclimatic change in East Asia: *Sedimentary Geology*, v. 364, p. 121–140, <https://doi.org/10.1016/j.sedgeo.2017.12.014>.
- Li, N., Chen, Y.J., Santosh, M., and Pirajno, F., 2015, Compositional polarity of Triassic granitoids in the Qinling Orogen, China: Implication for termination of the northernmost paleo-Tethys: *Gondwana Research*, v. 27, p. 244–257, <https://doi.org/10.1016/j.gr.2013.09.017>.
- Li, S., Zhao, S., Liu, X., Cao, H., Yu, S., Li, X., Somerville, I., Yu, S., and Suo, Y., 2018b, Closure of the proto-Tethys Ocean and early Paleozoic amalgamation of microcontinental blocks in east Asia: *Earth-Science Reviews*, v. 186, p. 37–75, <https://doi.org/10.1016/j.earscirev.2017.01.011>.
- Li, Y.Q., He, D.F., Li, D., Lu, R.Q., Fan, C., Sun, Y.P., and Huang, H.Y., 2018c, Sedimentary provenance constraints on the Jurassic to cretaceous paleogeography of Sichuan Basin, SW China: *Gondwana Research*, v. 60, p. 15–33, <https://doi.org/10.1016/j.gr.2018.03.015>.
- Li, Z., Kamp, P.J.J., Liu, S., Xu, G., Tong, K., Danisik, M., Wang, Z., Li, J., Deng, B., Ran, B., Ye, Y., and Wu, W., 2023, Late Cretaceous–Cenozoic thermal structure and exhumation of the Eastern Tibetan Plateau margin: A doubly-vergent orogenic wedge: *Earth-Science Reviews*, v. 238, <https://doi.org/10.1016/j.earscirev.2023.104319>.
- Li, Z.H., Lin, S.L., Cong, F., Xie, T., and Zou, G.F., 2012, U-Pb ages of zircon from metamorphic rocks of the Gaoligongshan Group in western Yunnan and its tectonic significance: *Acta Petrologica Sinica (Yanshi Xuebao)*, v. 28, p. 1529–1541.
- Liu, S., Li, Z., Kamp, P.J.J., Ran, B., and Li, X., 2019, Discovery of the Mesozoic Zoige paleo-plateau in eastern Tibetan plateau and its geological significance: *Journal of Chengdu University of Technology*, v. 46, p. 1–28 [in Chinese with English abstract].
- Liu, Y., Li, R.S., Ji, W.H., Pan, S.J., Chen, F.N., and Zhang, H.D., 2014, The pairing relationship between ophiolite and arc volcanic rocks along western Jinsha River suture zone and its geological significance: Evidence from geochemistry and LA-ICP-MS zircon U-Pb dating: *Dizhi Tongbao*, v. 33, p. 1076–1088 [in Chinese with English abstract].
- Liu-Zeng, J., Zhang, J., McPhillips, D., Reiners, P.W., Wang, W., Pik, R., Zeng, L., Hoke, G., Xie, K., Xiao, P., Zheng, D., and Ge, Y., 2018, Multiple episodes of fast exhumation since Cretaceous in southeast Tibet, revealed by low-temperature thermochronology: *Earth and Planetary Science Letters*, v. 490, p. 62–76, <https://doi.org/10.1016/j.epsl.2018.03.011>.
- Luo, A.B., Fan, J.J., Zhang, B.C., and Hao, Y.J., 2022, Cretaceous uplift history of the Tibetan Plateau: Insights from the transition of marine to terrestrial facies in central Tibet: *Palaeogeography, Palaeoclimatology, Palaeoecology*, v. 601, <https://doi.org/10.1016/j.palaeo.2022.111103>.
- Meng, E., Liu, F.L., Du, L.L., Liu, P.H., and Liu, J.H., 2015, Petrogenesis and tectonic significance of the Baoxing granitic and mafic intrusions, southwestern China: Evidence from zircon U-Pb dating and Lu-Hf isotopes, and whole-rock geochemistry: *Gondwana Research*, v. 28, p. 800–815, <https://doi.org/10.1016/j.gr.2014.07.003>.
- Meng, J., Wang, C., Zhao, X., Coe, R., Li, Y., and Finn, D., 2012, India-Asia collision was at 24°N and 50 Ma: Palaeomagnetic proof from southernmost Asia: *Scientific Reports*, v. 2, no. 925, <https://doi.org/10.1038/srep00925>.
- Meng, J., Coe, R.S., Wang, C., Gilder, S.A., Zhao, X., Liu, H., Li, Y., Ma, P., Shi, K., and Li, S., 2017, Reduced convergence within the Tibetan Plateau by 26 Ma?: *Geophysical Research Letters*, v. 44, p. 6624–6632, <https://doi.org/10.1002/2017GL074219>.
- Meng, J., Zhao, X., Wang, C., Liu, H., Li, Y., Han, Z., Liu, T., and Wang, M., 2018, Palaeomagnetism and detrital zircon U-Pb geochronology of Cretaceous redbeds from central Tibet and tectonic implications: *Geological Journal*, v. 53, p. 2315–2333, <https://doi.org/10.1002/gj.3070>.
- Meng, J., Gilder, S.A., Wang, C.S., Coe, R.S., Tan, X.D., Zhao, X.X., and He, K., 2019, Defining the limits of Greater India: *Geophysical Research Letters*, v. 46, p. 4182–4191, <https://doi.org/10.1029/2019GL082119>.
- Meng, J., Gilder, S.A., Li, Y.L., Wang, C.S., and Liu, T., 2020, Expansion of Greater India in the late Cretaceous: *Earth and Planetary Science Letters*, v. 542, <https://doi.org/10.1016/j.epsl.2020.116330>.
- Metcalfe, I., 2011, Tectonic framework and Phanerozoic evolution of Sundaland: *Gondwana Research*, v. 19, p. 3–21, <https://doi.org/10.1016/j.gr.2010.02.016>.
- Molnar, P., 2018, Simple concepts underlying the structure, support and growth of mountain ranges, high plateaus and other high terrain, *in* Hoorn, C., Perrigo, A., and Antonelli, A., eds., *Mountains, Climate and Biodiversity*: Hoboken, New Jersey, USA, Wiley-Blackwell, p. 17–36.
- Nguyen, T.A., Fyhn, M.B., Kristensen, J.A., Nielsen, L.H., Thomsen, T.B., Keulen, N., Sofie Lindström, S., and Bodreel, L.O., 2021, Provenance of the Phuquoc Basin fill, southern Indochina: Implication for Early Cretaceous drainage patterns and basin configuration in Southeast Asia: *Gondwana Research*, v. 98, p. 166–190, <https://doi.org/10.1016/j.gr.2021.03.014>.
- Nie, S.Y., Yin, A., Rowley, D.B., and Jin, Y., 1994, Exhumation of the Dabie Shan ultra-high-pressure rocks and accumulation of the Songpan-Ganzi flysch sequence, Central China: *Geology*, v. 22, p. 999–1002, [https://doi.org/10.1130/0091-7613\(1994\)022<0999:EOTDSU>2.3.CO;2](https://doi.org/10.1130/0091-7613(1994)022<0999:EOTDSU>2.3.CO;2).
- Qi, X.B., Wei, C., Cai, Z.H., Huang, M.H., Liu, Y.X., and Ji, F.B., 2019, Sedimentary age of metamorphic rocks of Gaoligong Group in Tengchong Block, Western Yunnan and its relationship with subduction/accretion of Proto-tethys: Evidences from detrital zircon u-pb dating and geochemistry: *Acta Geologica Sinica*, v. 93, p. 94–116 [in Chinese with English abstract].
- Rech, J.A., Currie, B.S., Jordan, T.E., Riquelme, R., and Gooley, J.T., 2019, Massive middle Miocene gypsic paleosols in the Atacama Desert and the formation of the central Andean rain-shadow: *Earth and Planetary Science Letters*, v. 506, p. 184–194, <https://doi.org/10.1016/j.epsl.2018.10.040>.
- Reid, A.J., Fowler, A.P., Phillips, D., and Wilson, C.J.L., 2005, Thermochronology of the Yidun Arc, central eastern Tibetan Plateau: Constraints from <sup>40</sup>Ar/<sup>39</sup>Ar K-feldspar and apatite fission track data: *Journal of Asian Earth Sciences*, v. 25, p. 915–935, <https://doi.org/10.1016/j.jseas.2004.09.002>.
- Rodríguez-López, J.P., and Wu, C.H., 2020, Recurrent deformations of aeolian desert dunes in the Cretaceous of the South China Block: Trigger mechanisms variability and implications for aeolian reservoirs: *Marine and Petroleum Geology*, v. 119, <https://doi.org/10.1016/j.marpetgeo.2020.104483>.
- Roger, F., Malavieille, J., and Leloup, P.H., 2004, Timing of granite emplacement and cooling in the Songpan-Garzê fold belt (eastern Tibetan plateau) with tectonic implications: *Journal of Asian Earth Sciences*, v. 22, p. 465–481, [https://doi.org/10.1016/S1367-9120\(03\)00089-0](https://doi.org/10.1016/S1367-9120(03)00089-0).
- Roger, F., Jolivet, M., and Malavieille, J., 2010, The tectonic evolution of the Songpan-Garzê (North Tibet) and adjacent areas from Proterozoic to Present: A synthesis: *Journal of Asian Earth Sciences*, v. 39, p. 254–269, <https://doi.org/10.1016/j.jseas.2010.03.008>.
- Ruddiman, W.F., and Kutzbach, J.E., 1989, Forcing of late Cenozoic northern hemisphere climate by plateau uplift in southern Asia and the American west: *Journal of Geophysical Research: Atmospheres*, v. 94, p. 18,409–18,427, <https://doi.org/10.1029/JD094iD15p18409>.
- Saylor, J.E., Jordan, J.C., Sundell, K.E., Wang, X., Wang, S., and Deng, T., 2018, Topographic growth of the Iishi Shan and its impact on basin and hydrology evolution: NE Tibetan Plateau: *Basin Research*, v. 30, p. 544–563, <https://doi.org/10.1111/bre.12264>.
- Schärer, U., Tapponnier, P., Lacassin, R., Leloup, P.H., Zhong, D.R., and Ji, S.C., 1990, Intraplate tectonics in Asia: A precise age for large-scale Miocene movement along the Ailao Shan-Red River shear zone, China:

- Earth and Planetary Science Letters, v. 97, p. 65–77, [https://doi.org/10.1016/0012-821X\(90\)90099-J](https://doi.org/10.1016/0012-821X(90)90099-J).
- Scotese, C.R., 2002, Paleomap Project, <http://www.scotese.com> (accessed 5.01.2014).
- Şengör, A.M.C., 1985, Geology: East Asian tectonic collage: *Nature*, v. 318, no. 6041, p. 16–17, <https://doi.org/10.1038/318016a0>.
- Shellnutt, J.G., 2014, The Emeishan large igneous province: A synthesis: *Geoscience Frontiers*, v. 5, p. 369–394, <https://doi.org/10.1016/j.gsf.2013.07.003>.
- Shi, X.H., 2015, Characteristics of nappe structures and the basin-range coupling in the middle of southwest of Lanping Basin [Master dissertation]: Chengdu, China, Chengdu University of Technology, [in Chinese with English abstract].
- Spicer, R.A., Su, T., Valdes, P.J., Farnsworth, A., Wu, F.X., Shi, G., Spicer, T.V., and Zhou, Z., 2021, Why ‘the uplift of the Tibetan Plateau’ is a myth: *National Science Review*, v. 8, no. 1, <https://doi.org/10.1093/nsr/nwaa091>.
- Sun, J.M., Ye, J., Wu, W., Ni, X., Bi, S., Zhang, Z., Liu, W., and Meng, J., 2010, Late Oligocene–Miocene mid-latitude aridification and wind patterns in the Asian interior: *Geology*, v. 38, p. 515–518, <https://doi.org/10.1130/G30776.1>.
- Sun, J.M., Zheng, Z.L., Cao, M.M., Windley, B., Tian, S.C., Sha, J.G., Abdulov, S., Gadoev, M., and Oimhamadov, I., 2020, Timing of seaway retreat from proto-Paratethys, sedimentary provenance, and tectonic rotations in the late Eocene-early Oligocene in the Tajik Basin, Central Asia: *Palaeogeography, Palaeoclimatology, Palaeoecology*, v. 545, <https://doi.org/10.1016/j.palaeo.2020.109657>.
- Sundell, K.E., and Saylor, J.E., 2017, Unmixing detrital geochronology age distributions: *Geochemistry, Geophysics, Geosystems*, v. 18, p. 2872–2886, <https://doi.org/10.1002/2016GC006774>.
- Suo, Y., Li, S., Jin, C., Zhang, Y., and Somerville, I., 2019, Eastward tectonic migration and transition of the Jurassic–Cretaceous Andean-type continental margin along southeast China: *Earth-Science Reviews*, v. 196, <https://doi.org/10.1016/j.earscirev.2019.102884>.
- Tapponnier, P., et al., 1981, The Tibetan side of the India–Eurasia collision: *Nature*, v. 294, p. 405–410, <https://doi.org/10.1038/294405a0>.
- Tapponnier, P., Zhiqin, X., Roger, F., Meyer, B., Arnaud, N., Wittlinger, G., and Jingsui, Y., 2001, Oblique stepwise rise and growth of the Tibet Plateau: *Science*, v. 294, p. 1671–1677, <https://doi.org/10.1126/science.105978>.
- Tian, Y., Kohn, B.P., Zhu, C., Xu, M., Hu, S., and Gleadow, A.J.W., 2012, Post-orogenic evolution of the Mesozoic Miao Wang Shan Foreland Basin system, central China: *Basin Research*, v. 24, p. 70–90, <https://doi.org/10.1111/j.1365-2117.2011.00516.x>.
- Tian, Y., Kohn, B.P., Gleadow, A.J.W., and Hu, S., 2014a, A thermochronological perspective on the morphotectonic evolution of the southeastern Tibetan Plateau: *Journal of Geophysical Research: Solid Earth*, v. 119, p. 676–698, <https://doi.org/10.1002/2013JB010429>.
- Tian, Y., Kohn, B.P., Hu, S., and Gleadow, A.J.W., 2014b, Postorogenic rigid behavior of the eastern Songpan-Ganze terrane: Insights from low-temperature thermochronology and implications for intracontinental deformation in central Asia: *Geochemistry, Geophysics, Geosystems*, v. 15, p. 453–474, <https://doi.org/10.1002/2013GC004951>.
- Tong, Y.B., Yang, Z., Zheng, L.D., Xu, Y.L., Wang, H., Gao, L., and Hu, X.Z., 2013, Internal crustal deformation in the northern part of Shan-Thai Block: New evidence from paleomagnetic results of Cretaceous and Paleogene redbeds: *Tectonophysics*, v. 608, p. 1138–1158, <https://doi.org/10.1016/j.tecto.2013.06.031>.
- van Hinsbergen, D.J.J., Lippert, P.C., Dupont-Nivet, G., McQuarrie, N., Doubrovine, P.V., Spakman, W., and Torsvik, T.H., 2012, Greater India Basin hypothesis and a two-stage Cenozoic collision between India and Asia: *Proceedings of the National Academy of Sciences*, v. 109, p. 7659–7664, <https://doi.org/10.1073/pnas.1117262109>.
- Wang, C., Zhao, X., Liu, Z., Lippert, P.C., Graham, S.A., Coe, R.S., Yi, H., Zhu, L., Liu, S., and Li, Y., 2008, Constraints on the early uplift history of the Tibetan Plateau: *Proceedings of the National Academy of Sciences*, v. 105, p. 4987–4992, <https://doi.org/10.1073/pnas.0703595105>.
- Wang, L., Liu, C., Fei, M., Shen, L., Zhang, H., and Zhao, Y., 2015, First SHRIMP U-Pb zircon ages of the potash-bearing Mengyejing formation, Simao Basin, southwestern Yunnan, China: *Cretaceous Research*, v. 52, p. 238–250, <https://doi.org/10.1016/j.cretres.2014.09.008>.
- Wang, L., Garzanti, E., Cai, F., Zhang, J., Shen, L., Nulay, P., Siritongkham, N., Ding, L., and Wang, C., 2023, The underestimated role of tectonics in the mid-Late Cretaceous desertification in SE Asia: *Geological Society of America Bulletin* (in press), <https://doi.org/10.1130/B36839.1>.
- Wang, L.C., Shen, L.J., Liu, C.L., Chen, K., Ding, L., and Wang, C.S., 2021, The Late Cretaceous source-to-sink system at the eastern margin of the Tibetan Plateau: Insights from the provenance of the Lanping Basin: *Geoscience Frontiers*, v. 12, 101102, <https://doi.org/10.1016/j.gsf.2020.11.002>.
- Wang, P.X., 1998, Deformation of Asia and global cooling: Searching links between climate and tectonics: *Quaternary Sciences*, v. 3, p. 213–221 [in Chinese with English abstract].
- Wang, X., Carrapa, B., Chapman, J.B., Henriquez, S., Wang, M., DeCelles, P.G., Li, Z., Wang, F., Oimhamadov, I., Gadoev, M., and Chen, F., 2019, Paratethys last gasp in central Asia and late Oligocene accelerated uplift of the Pamirs: *Geophysical Research Letters*, v. 46, no. 21, p. 11,773–11,781, <https://doi.org/10.1029/2019GL084838>.
- Wang, X.S., Bi, X.W., Leng, C.B., Zhong, H., Tang, H.F., Chen, Y.W., Yin, G.H., Ding-Zhu Huang, D.Z., and Zhou, M.F., 2014, Geochronology and geochemistry of late Cretaceous igneous intrusions and Mo-Cu-(W) mineralization in the southern Yidun arc, SW China: Implications for metallogenesis and geodynamic setting: *Ore Geology Reviews*, v. 61, p. 73–95, <https://doi.org/10.1016/j.oregeorev.2014.01.006>.
- Wang, X.Y., 2021, Meso-Cenozoic cooling history of the Western Qinling [M.A. thesis]: Constraints from low-temperature thermochronology: Beijing, China, China University of Geosciences, 66 p.
- Wang, X.Y., Wang, S.F., Wang, C., and Chen, L.Y., 2017, LA-ICP-MS zircon U-Pb age, geochemistry and tectonic significance of Late Triassic granites in Jinshajiang belt of Batang area, eastern Tibet: *Chinese Journal of Geology*, v. 52, p. 1160–1180 [in Chinese with English abstract].
- Wang, Y., Zhang, A., Fan, W., Peng, T., Zhang, F., Zhang, Y., and Bi, X., 2010, Petrogenesis of late Triassic post-collisional basaltic rocks of the Lancangjiang tectonic zone, southwest China, and tectonic implications for the evolution of the eastern Paleotethys: *Geochronological and geochemical constraints: Lithos*, v. 120, p. 529–546, <https://doi.org/10.1016/j.lithos.2010.09.012>.
- Weislogel, A.L., 2008, Tectonostratigraphic and geochronologic constraints on evolution of the northeast Paleotethys from the Songpan-Ganzi complex, central China: *Tectonophysics*, v. 451, p. 331–345, <https://doi.org/10.1016/j.tecto.2007.11.053>.
- Weislogel, A.L., Graham, S.A., Chang, E.Z., Wooden, J.L., Gehrels, G.E., and Yang, H.S., 2006, Detrital zircon provenance of the Late Triassic Songpan-Ganzi complex: Sedimentary record of collision of the North and South China blocks: *Geology*, v. 34, p. 97–100, <https://doi.org/10.1130/G21929.1>.
- Weislogel, A.L., Graham, S.A., Chang, E.Z., Wooden, J.L., and Gehrels, G.E., 2010, Detrital zircon provenance from three turbidite depocenters of the Middle–Upper Triassic Songpan-Ganzi complex, central China: Record of collisional tectonics, erosional exhumation, and sediment production: *Geological Society of America Bulletin*, v. 122, p. 2041–2062, <https://doi.org/10.1130/B26606.1>.
- Wilson, C.J.L., and Fowler, A.P., 2011, Denudational response to surface uplift in east Tibet: Evidence from apatite fission-track thermochronology: *Geological Society of America Bulletin*, v. 123, p. 1966–1987, <https://doi.org/10.1130/B30331.1>.
- Wu, C., Rodríguez-López, J.P., and Santosh, M., 2022, Plateau archives of lithosphere dynamics, cryosphere and paleoclimate: The formation of Cretaceous desert basins in east Asia: *Geoscience Frontiers*, v. 13, <https://doi.org/10.1016/j.gsf.2022.101454>.
- Wu, C.H., and Rodríguez-López, J.P., 2021, Cryospheric processes in Quaternary and Cretaceous hyper-arid plateau desert oases: *Sedimentology*, v. 68, p. 755–770, <https://doi.org/10.1111/sed.12804>.
- Wu, C.H., Liu, C.L., Yi, H.S., Xia, G.Q., Zhang, H., Wang, L.C., Li, G.J., and Wagerich, M., 2017, Mid-Cretaceous desert system in the Simao Basin, southwestern China, and its implications for sea-level change during a greenhouse climate: *Palaeogeography, Palaeoclimatology, Palaeoecology*, v. 468, p. 529–544, <https://doi.org/10.1016/j.palaeo.2016.12.048>.
- Wu, C.H., Rodríguez-López, J.P., Liu, C., Sun, X., Wang, J., Xia, G., and Wagerich, M., 2018, Late Cretaceous climbing erg systems in the western Xinjiang Basin: Palaeoatmosphere dynamics and East Asia margin tectonic forcing on desert expansion and preservation: *Marine and Petroleum Geology*, v. 93, p. 539–552, <https://doi.org/10.1016/j.marpetgeo.2018.03.038>.
- Xiao, L., Zhang, H.F., Clemens, J.D., Wang, Q.W., Kan, Z.Z., Wang, K.M., Ni, P.Z., and Liu, X.M., 2007, Late Triassic granitoids of the eastern margin of the Tibetan Plateau: Geochronology, petrogenesis and implications for tectonic evolution: *Lithos*, v. 96, p. 436–452, <https://doi.org/10.1016/j.lithos.2006.11.011>.
- Xin, D., Yang, T., Xue, C., Liao, C., Han, X., Liang, M., and Li, X., 2018, The Carboniferous strata in the Fugong region, Western Yunnan likely belong to the Lhasa terrane: Evidence from detrital zircon U-Pb age-spectra: *Acta Petrologica Sinica (Yanshi Xuebao)*, v. 34, p. 1335–1346 [in Chinese with English abstract].
- Xu, Y.F., Liu, J.P., Cong, F., Sun, B.D., and Huang, X.M., 2018, LA-ICP-MS zircon U-Pb dating of the Chongshan Group in the Xiaowan area along the southern section of the Lancang River in western Yunnan and its geological significance: *Dizhi Tongbao*, v. 37, p. 1006–1014 [in Chinese with English abstract].
- Xu, Z.Q., et al., 2016, Review of “Orogenic plateau”: *Acta Petrologica Sinica (Yanshi Xuebao)*, v. 32, p. 3557–3571 [in Chinese with English abstract].
- Yan, M., Zhang, D., Fang, X., Zhang, W., Song, C., Liu, C., Zan, J., and Shen, M., 2021, New insights on the age of the Mengyejing Formation in the Simao Basin, SE Tethyan domain and its geological implications: *Science China: Earth Sciences*, v. 64, p. 231–252, <https://doi.org/10.1007/s11430-020-9689-3>.
- Yin, A., and Harrison, T.M., 2000, Geologic evolution of the Himalayan-Tibetan orogen: *Annual Review of Earth and Planetary Sciences*, v. 28, no. 1, p. 211–280, <https://doi.org/10.1146/annurev.earth.28.1.211>.
- Yin, J.Y., Sun, Z.M., Yang, Z.Y., and Liang, Q.Z., 1999, Cretaceous and early Tertiary paleomagnetic results from the Lanping Basin and its geological implications: *Chinese Journal of Geophysics*, v. 42, p. 648–659 [in Chinese with English abstract].
- Yuan, C., Zhou, M.F., Sun, M., Zhao, Y.J., Wilde, S., Long, X.P., and Yan, D.P., 2010, Triassic granitoids in the eastern Songpan Ganzi Fold Belt, SW China: Magmatic response to geodynamics of the deep lithosphere: *Earth and Planetary Science Letters*, v. 290, p. 481–492, <https://doi.org/10.1016/j.epsl.2010.01.005>.
- Yuan, Q., Qin, Z.J., Wei, H.C., Sheng, S.R., and Shan, F.S., 2013, The ore-forming age and palaeoenvironment of the Mengyejing Formation in Jiangcheng, Yunnan Province: *Acta Geoscientia Sinica*, v. 34, p. 631–637 [in Chinese with English abstract], <https://doi.org/10.3975/cagsb.2013.05.15>.
- Zhang, H.F., Zhang, L., Harris, N.J., Jin, L.L., and Yuan, H.L., 2006, U-Pb zircon ages, geochemical and isotopic compositions of granitoids in Songpan-Garze fold belt, eastern Tibetan Plateau: Constraints on petrogenesis and tectonic evolution of the basement: *Contributions to Mineralogy and Petrology*, v. 152, p. 75–88, <https://doi.org/10.1007/s00410-006-0095-2> [in Chinese with English abstract].
- Zhang, H.P., Oskin, M.E., Liu-Zeng, J., Zhang, P., Reiners, P.W., and Xiao, P., 2016, Pulsed exhumation of inte-

- rior eastern Tibet: Implications for relief generation mechanisms and the origin of high-elevation planation surfaces: *Earth and Planetary Science Letters*, v. 449, p. 176–185, <https://doi.org/10.1016/j.epsl.2016.05.048>.
- Zhao, X.D., Zhang, H.P., Hetzel, R., Kirby, E., Duvall, A.R., Whipple, K.X., Xiong, J.G., Li, Y.F., Pang, J.Z., Wang, Y., Wang, P., Liu, K., Ma, P.F., Zhang, B., Li, X.M., Zhang, J.W., and Zhang, P.Z., 2021, Existence of a continental-scale river system in eastern Tibet during the late Cretaceous–early Paleogene: *Nature Communications*, v. 12, 7231, <https://doi.org/10.1038/s41467-021-27587-9>.
- Zheng, H.B., 2015, Birth of the Yangtze River: Age and tectonic-geomorphic implications: *National Science Review*, v. 2, p. 438–453, <https://doi.org/10.1093/nsr/nwv063>.
- Zhu, M., Chen, H.L., Zhou, J., and Yang, S.F., 2017, Provenance change from the Middle to Late Triassic of the southwestern Sichuan basin, Southwest China: Constraints from the sedimentary record and its tectonic significance: *Tectonophysics*, v. 700–701, p. 92–107, <https://doi.org/10.1016/j.tecto.2017.02.006>.

SCIENCE EDITOR: WENJIAO XIAO  
ASSOCIATE EDITOR: XIXI ZHAO

MANUSCRIPT RECEIVED 13 SEPTEMBER 2022  
REVISED MANUSCRIPT RECEIVED 1 JULY 2023  
MANUSCRIPT ACCEPTED 24 JULY 2023

Printed in the USA